

Recent developments in chiral and spin polarization effects in heavy-ion collisionsJian-Hua Gao,^{1,*} Guo-Liang Ma,^{2,†} Shi Pu,^{3,‡} and Qun Wang^{3,§}¹*Shandong Key Laboratory of Optical Astronomy and Solar-Terrestrial Environment, School of Space Science and Physics, Institute of Space Sciences, Shandong University, Weihai 264209, China*²*Key Laboratory of Nuclear Physics and Ion-beam Application (MOE), Institute of Modern Physics, Fudan University, Shanghai 200433, China*³*Department of Modern Physics, University of Science and Technology of China, Hefei 230026, China*

We give a brief overview of recent theoretical and experimental results on the chiral magnetic effect and spin polarization effect in heavy-ion collisions. We present updated experimental results for the chiral magnetic effect and related phenomena. The time evolution of the magnetic fields in different models is discussed. The newly developed quantum kinetic theory for massive fermions is reviewed. We present theoretical and experimental results for the polarization of Λ hyperons and the ρ_{00} value of vector mesons.

Keywords: Relativistic Heavy-Ion Collisions, Chiral Magnetic Effect, Chiral Kinetic Theory, Spin Polarization

I. INTRODUCTION

In relativistic heavy-ion collisions, two charged nuclei collide to produce a hot, dense state of matter known as a quark-gluon plasma (QGP). Very high magnetic fields and orbital angular momenta (OAMs) are generated in these collisions. The magnetic fields are on the order of 10^{17-18} Gs [1–4] and are the strongest magnetic fields observed in nature. The QGP is also found to be the most vortical fluid [5], where a huge OAM is transferred to the fluid in the form of vorticity fields. These novel phenomena open a new window for the study of the QGP in heavy-ion collisions. These novel phenomena are quantum in nature and are usually negligible in classical fluids.

The chiral magnetic effect (CME) and chiral separation effect (CSE) [6–8] are two quantum effects on the magnetic field in a chiral fermion system. In the CME, a charge current is induced along the magnetic field:

$$\mathbf{j} = \frac{e^2}{2\pi^2} \mu_5 \mathbf{B}, \quad (1)$$

where μ_5 is the chiral chemical potential. The magnetic field can also generate a chiral current

$$\mathbf{j}_5 = \frac{e^2}{2\pi^2} \mu \mathbf{B}, \quad (2)$$

where μ is the charge chemical potential. These two quantum effects are related to the chiral anomaly, which is absent from classical theories. The chiral chemical potential represents a chirality imbalance. The nonzero μ_5 arises from topological fluctuations in quantum chromodynamics (QCD), which are related to the local violation of parity and charge parity. Therefore, the observation of the CME in heavy-ion collisions implies local parity and charge parity violation. The collective modes associated with the CME and CSE are called the chiral magnetic wave (CMW). In addition, the CME has been observed in condensed matter [9] and can be applied in quantum computing [10]. These phenomena are discussed in more detail in recent reviews [11–20] and references therein.

In non-central heavy-ion collisions, part of the very large OAM of colliding nuclei is converted to a vorticity field in the fluid. The vorticity can be regarded as the local OAM of the fluid and can polarize particles with spins through spin-orbit coupling. The global spin polarization of particles is along the direction of the global OAM of colliding nuclei (or the direction perpendicular to the reaction plane). The global polarization of Λ and $\bar{\Lambda}$ hyperons has been measured in the STAR experiment, and the average angular velocity or vorticity was estimated as $\omega \sim 10^{22} s^{-1}$ [5]. The data on the global polarization of Λ and $\bar{\Lambda}$ hyperons can be well described by various phenomenological models.

The STAR Collaboration has also measured the local spin polarization effect in Au+Au collisions at 200 GeV [21]. The data show a decreasing trend from in-plane to out-of-plane for the global spin polarization. In addition, the STAR Collaboration measured the azimuthal angle dependence of the spin polarization along the beam direction. These experimental results are still difficult to understand in terms of phenomenological models.

* Corresponding author, gaojh@sdu.edu.cn

† Corresponding author, glma@fudan.edu.cn

‡ Corresponding author, shipu@ustc.edu.cn

§ Corresponding author, qunwang@ustc.edu.cn

This paper is structured as follows. In Sec. II A, we review recent progress in theoretical studies of the CME and related effects in heavy-ion collisions. In Sec. II B, we present experimental results on the CME and CMW. In Sec. III, we give a brief overview of recent developments in the quantum kinetic theory for massive fermions. In Sec. IV A, we discuss the decomposition of the OAM and spin from the total angular momentum as well as the spin hydrodynamics. In Sec. IV B, we discuss experimental results on the global and local polarization effects and spin alignments of vector mesons. We summarize the paper in Sec. V.

II. CHIRAL MAGNETIC AND RELATED EFFECTS IN HEAVY-ION COLLISIONS

A. Theoretical progress

To study the magnetic-field-related effects in heavy-ion collisions, we need to know the magnetic field as a function of time. The electromagnetic field can be estimated using the Lienard–Wiechert potential [1–4]. Although the peak value of the magnetic field can be as large as a few times m_π^2 , where m_π is the mass of a pion, it decays very rapidly in vacuum [7]. Such a magnetic field in vacuum could not provide sufficient time to generate the CME and other chiral transport effects; thus, intermediate effects must be present [4, 22–24].

Magnetohydrodynamics (MHD) is widely used in astrophysics to investigate the coupling between a charged medium and a magnetic field. Ordinary MHD consists of the hydrodynamic conservation equations coupled with Maxwell’s equations. Very recently, several MHD studies [25–29] showed that the magnetic fields decay as $1/\tau$ in the infinite electrical conductivity limit, where τ is the proper time. The analytic solution for the anomalous MHD with the CME and chiral anomaly in a Bjorken flow has been derived [30, 31]. The magnetic fields decay approximately as $\sim 1/\tau$ or $\sim e^{-\sigma\tau}/\tau$, where σ is the electrical conductivity. For numerical simulations of the ideal MHD, see Ref. [32, 33]. Although the electrical conductivity of the QGP is not infinite, it is important to study the coupling between the electromagnetic field and QGP. The ratio of the magnetic density to the initial fluid density can reportedly be greater than 1 in event-by-event simulations of $\sqrt{s_{NN}} = 200$ GeV Au+Au collisions [3]; i.e., the magnetic field may also affect other physical quantities [25, 29, 34]. Further study of the relativistic MHD with a temperature-dependent electrical conductivity is needed.

The ideal MHD framework has been extended to the second order using the self-consistent Grad moment expansion [35, 36]. In this framework, the electromagnetic fields are coupled with normal dissipative terms, such as the shear viscous tensor and bulk viscous pressure. One can also use a similar approach based on the kinetic theory of massless fermions [37].

By comparing phenomenological studies and experimental data, one can constrain the lifetime of the magnetic field, $t_B \simeq 0.5 - 1$ fm/c [38] or $t_B = A/\sqrt{s_{NN}}$, where $A = 115 \pm 16$ GeV · fm/c [39].

It has been proposed that the magnetic field can be produced by a charged rotating fluid [39]. By using Maxwell’s equations in a charged fluid, $\partial_\mu F^{\mu\nu} = j^\nu$, and assuming the particle number density n is homogeneous or changes very slowly, the relationship between the vorticity and the magnetic field in the local rest frame, $\omega = (\nabla^2 B)/en$, can be obtained. By introducing the average vorticity $\bar{\omega}$, the average magnetic field per transverse area can be expressed as $\bar{B} \simeq \frac{e^2}{4\pi} An\bar{\omega}$, where A is the transverse area of the vortex. In heavy-ion collisions, the evolution of both the vorticity and the charge density at freeze-out can be extracted from AMPT simulations. (The AMPT model is a very good tool for simulating the CME [40–44]; see Sec. II B.) For a transverse area of the vorticity of 16π fm², and assuming a centrality of 20–50% for Au+Au collisions at 10–200 GeV at the RHIC, the magnetic field and its evolution can be estimated. Then, the splitting in the polarization of Λ and $\bar{\Lambda}$ hyperons can be estimated from the averaged magnetic field, $P_\Lambda - P_{\bar{\Lambda}} \simeq 2|\mu_\Lambda|\bar{B}/T_{fo}$, where $|\mu_\Lambda| = 0.613e/(2M_N)$, $M_N = 938$ MeV, and $T_{fo} = 155$ MeV. The numerical results are close to the STAR data [5].

Another theoretical model is the anomalous-viscous fluid dynamics (AVFD) [45–47], which is the hydrodynamical realization of the CME in relativistic heavy-ion collisions. The latest event-by-event version of the AVFD includes the local charge conservation (LCC) effect [48] and the introduction of particlization, which may be the best way to quantify the LCC [49]. It also gives predictions for isobaric collisions [50]. For the event plane, AVFD predicts $\zeta_{isobar}^{EP} \equiv \gamma_{Ru-Zr}^{OS-SS}|_{EP} / \delta_{Ru-Zr}^{OS-SS}|_{EP} \simeq -(0.41 \pm 0.27)$, which yields $\langle \cos(2\Psi_B - 2\Psi_{EP}) \rangle \simeq -0.46$; for the reaction plane, $\zeta_{isobar}^{RP} \equiv \gamma_{Ru-Zr}^{OS-SS}|_{RP} / \delta_{Ru-Zr}^{OS-SS}|_{RP} \simeq -(0.90 \pm 0.45)$, which yields $\langle \cos(2\Psi_B - 2\Psi_{RP}) \rangle \simeq -0.95$. According to the calculations, these ratios are independent of the initial axial charge.

As a natural extension to the CME, it is interesting to consider how large the mass correction is. This question can be addressed using a perturbation method in quantum kinetic theory, as described in Sec. III. However, as noted in Ref. [51], the mass correction to the CME is related to another well-known phenomenon, Schwinger pair production. The operator equation for the CME with finite mass corrections is the axial Ward identity,

$$\partial_\mu j_5^\mu = 2im\bar{\psi}\gamma^5\psi - \frac{e^2}{16\pi^2}\epsilon^{\mu\nu\alpha\beta}F_{\mu\nu}F_{\alpha\beta}. \quad (3)$$

To simplify the discussion, one can assume that the electric and magnetic fields E and B , respectively, are constant and homogeneous in the z direction. In this case, the theory reduces to a (1+1)-dimensional problem; therefore, it can be computed using the

worldline formalism. However, the original calculation by Schwinger [52] provides only the value of $\langle \text{out}, 0 | \partial_\mu j_5^\mu | \text{in}, 0 \rangle = 0$, where $|\text{in}, 0\rangle$ and $|\text{out}, 0\rangle$ are the in and out states in vacuum, respectively. One needs to compute the expectation values of all the operators in (3); i.e., one needs to compute $\langle \text{in}, 0 | \partial_\mu j_5^\mu | \text{in}, 0 \rangle$. The method of computing the Feynman propagator in the in-in state has been used to obtain the following result by a long and technical calculation [53]:

$$\partial_\mu j_5^\mu = \frac{e^2 EB}{2\pi^2} \exp\left(-\frac{\pi m^2}{eE}\right), \quad (4)$$

which reduces to the standard chiral anomaly, $\partial_\mu j_5^\mu = e^2 EB/(2\pi^2)$, in the massless limit. It is also consistent with the physical scenario suggested in Ref. [51], which implies that the chirality production rate should be proportional to the Schwinger pair production rate. In addition, several other physical quantities can also be obtained by the real-time worldline formalism. The mass-corrected CME current is given by

$$j^z = \frac{e^2 EB}{2\pi^2} \coth\left(\frac{B}{E}\pi\right) \exp\left(-\frac{\pi m^2}{eE}\right), \quad (5)$$

where the factor $\coth(B\pi/E)$ represents the sum over the Landau levels.

There are also many studies of the anomaly and CME in the context of perturbation in quantum field theory [54–58]. The source of the CME, the chiral charge fluctuation [59, 60], is another research topic and is important for determining the magnitude of the CME signal.

B. Recent experimental results

The dipole charge separation due to the CME can be characterized by the first sine term a_1 in the Fourier series of the charged-particle azimuthal distribution:

$$\frac{dN}{d\phi} \propto 1 + 2 \sum_n \left\{ v_n \cos[n(\phi - \Psi_{RP})] + a_n \sin[n(\phi - \Psi_{RP})] \right\}, \quad (6)$$

where $\phi - \Psi_{RP}$ represents the particle azimuthal angle with respect to the reaction plane angle Ψ_{RP} in heavy-ion collisions (which is determined by the impact parameter and beam axis), and v_n and a_n are the coefficients of the P -even and P -odd Fourier terms, respectively. An azimuthal three-particle correlator [61], γ_{112} , was proposed to explore the first coefficient, a_1 , of the P -odd Fourier terms characterizing the charge separation due to the CME; it is given by

$$\gamma_{112} \equiv \langle \cos(\phi_\alpha + \phi_\beta - 2\Psi_{RP}) \rangle \simeq \langle \cos(\phi_\alpha + \phi_\beta - 2\Psi_2) \rangle, \quad (7)$$

where α and β denote particles with the same or opposite electric charge, respectively; angle brackets denote the averages over particles and events, and Ψ_{RP} can be approximated by the azimuthal angle of the second-order event plane, Ψ_2 . Similarly, γ_{123} , a charge-dependent correlator with respect to the azimuthal angle of the third-order event plane, Ψ_3 , is defined as

$$\gamma_{123} \equiv \langle \cos(\phi_\alpha + 2\phi_\beta - 3\Psi_3) \rangle \quad (8)$$

and can reflect the charge-dependent background effects unrelated to the CME, because Ψ_3 is not correlated with the magnetic field direction. Other types of azimuthal correlators γ_{ijk} for charged particles can also be defined similarly for different purposes. Except in ambiguous cases, we use the shorthand notation γ to represent γ_{112} hereafter.

From the CME expectation, the difference between the opposite-sign and same-sign correlation for charged particles $\Delta\gamma = \gamma_{\text{opp}} - \gamma_{\text{same}}$ is expected to be proportional to B^2 and $\cos[2(\Psi_B - \Psi_2)]$ [1, 42, 64]:

$$\Delta\gamma \propto \langle B^2 \cos[2(\Psi_B - \Psi_2)] \rangle. \quad (9)$$

Because the magnitude of the magnetic field is proportional to the collision energy [2, 65], the CME should produce large differences between the γ correlators at very different energies, such as the RHIC and LHC energies. However, Fig. 1 shows a very weak energy dependence of the γ correlator in a wide energy range from the RHIC energy to the LHC energy.

As (9) shows, the $\Delta\gamma$ resulting from the CME is proportional to both the squared magnetic field and the correlation in the magnetic field direction with respect to the event plane. The left panel of Fig. 2 shows the simulation results of $\Delta\gamma$ due to the CME as a function of the centrality for Pb+Pb collisions at 5.02 TeV and Xe+Xe collisions at 5.44 TeV. They are very different except in the most central collisions. However, the right panel of Fig. 2 shows the preliminary ALICE data for Xe+Xe collisions,

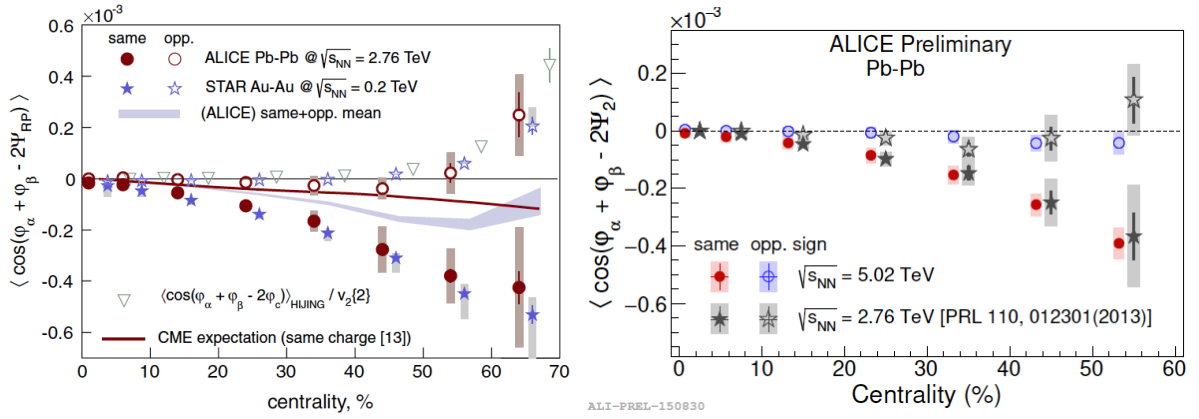


Fig. 1. Measured centrality dependence of the γ_{112} correlator for Au+Au collisions at 200 GeV and Pb+Pb collisions at 2.76 TeV [62] (left panel) and for Pb+Pb collisions at 2.76 TeV and 5.02 TeV (right panel) [63].

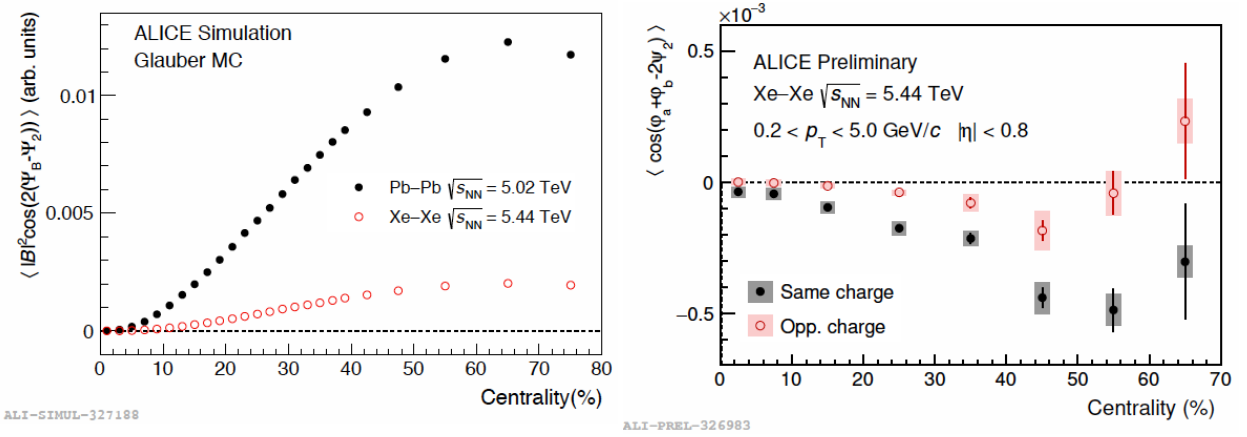


Fig. 2. Results of simulation of $\Delta\gamma$ as a function of centrality for the CME in Pb+Pb collisions at 5.02 TeV and Xe+Xe collisions at 5.44 TeV (left panel); ALICE measurements of the γ_{112} correlator for Xe+Xe collisions at 5.44 TeV (right panel) [63].

which show a centrality dependence that is very similar to that for Pb+Pb collisions in Fig. 1. The observed weak independence of $\Delta\gamma$ from the collision energy indicates that the dominant component of $\Delta\gamma$ is most likely due to the background.

One may argue, however, that the CME signal also depends on the lifetime of the magnetic field. Because of the shorter magnetic field lifetime at higher collision energies, the signal is very weak at very high energies. Fortunately, experimentalists are searching for a possible signal by comparing Au+Au collisions and U+U collisions at the RHIC. The top-left panel of Fig. 3 shows the expected CME contribution to $\Delta\gamma$ as a function of N_{part} for Au+Au collisions at 200 GeV and U+U collisions at 193 GeV [66], which are multiplied by a factor $N_{\text{part}}/\epsilon_n$ to scale the effect from the elliptic flow and transverse momentum conservation. The CME contributions for Au+Au and U+U collisions are different except in very peripheral collisions. The difference is sizable for N_{part} larger than 150. In addition, the background contribution to $\Delta\gamma$ is simulated using a hydrodynamics model with and without maximal LCC, as shown in the bottom-left panel of Fig. 3. For each case, the expected contribution is almost the same for Au+Au collisions at 200 GeV and U+U collisions at 193 GeV, although local charge conservation can significantly increase the magnitude of $\Delta\gamma$. To check these results, the STAR Collaboration has measured three correlators, $\Delta\gamma_{112}$, $\Delta\gamma_{123}$, and $\Delta\gamma_{132}$, in Au+Au collisions at 200 GeV and U+U collisions at 193 GeV [66]. Their N_{part} dependence is presented in the right panel of Fig. 3; they are normalized by a factor of N_{part}/v_n for the above reason. It is observed that the mixed harmonic correlations do not follow the background-only expectations. Differences between these correlators in Au+Au collisions and U+U collisions appear only for very central collisions with N_{part} larger than 300. The illustrations on the far right side of Fig. 3 show that $\Delta\gamma_{123}$ is not correlated with the magnetic field direction, in contrast to $\Delta\gamma_{112}$ and $\Delta\gamma_{132}$; it is hard to see whether this difference is due to the signal or the background. A detailed study of these correlators is needed to clarify their nature.

To extract the contribution of the CME to the observable $\Delta\gamma$, the $\Delta\gamma$ measured in the STAR experiment was decomposed

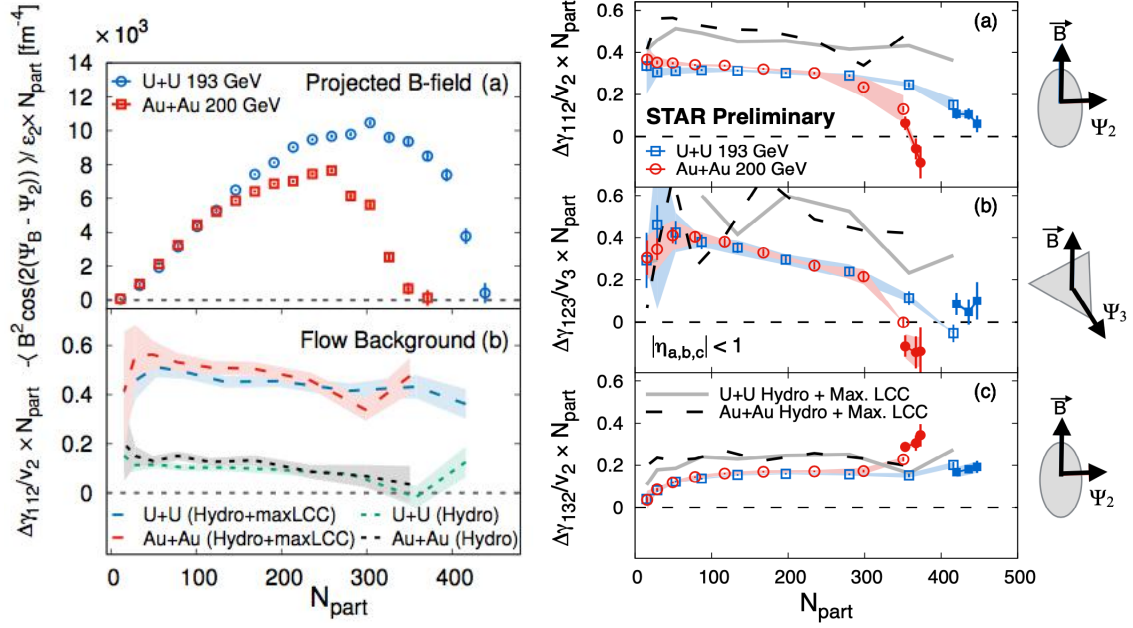


Fig. 3. N_{part} dependence of the CME contribution (top left) and flow background (bottom left) projected onto the correlator γ_{112} for Au+Au collisions at 200 GeV and U+U collisions at 193 GeV. STAR measurements of N_{part} dependence of the correlators ($\Delta\gamma_{112}$, $\Delta\gamma_{123}$, and $\Delta\gamma_{132}$) multiplied by a factor of N_{part}/v_n for Au+Au collisions at 200 GeV and U+U collisions at 193 GeV (right panel) [66].

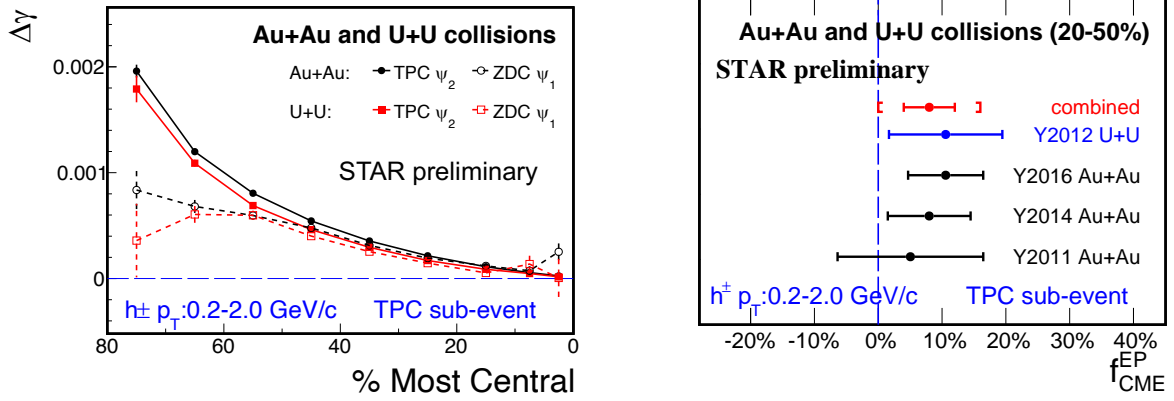


Fig. 4. STAR measurements of the centrality dependence of $\Delta\gamma_{112}$ with respect to the ZDC and TPC event planes (left panel) and extracted CME fractions $f_{\text{CME}}^{\text{EP}}$ (right panel) from Au+Au collisions at 200 GeV and U+U collisions at 193 GeV [66].

into the v_2 background and the CME signal:

$$\begin{aligned}\Delta\gamma(\psi_{\text{TPC}}) &= \Delta\gamma_{\text{CME}}(\psi_{\text{TPC}}) + \Delta\gamma_{\text{Bkg}}(\psi_{\text{TPC}}), \\ \Delta\gamma(\psi_{\text{ZDC}}) &= \Delta\gamma_{\text{CME}}(\psi_{\text{ZDC}}) + \Delta\gamma_{\text{Bkg}}(\psi_{\text{ZDC}}),\end{aligned}\quad (10)$$

where ψ_{TPC} and ψ_{ZDC} are the event planes measured for mid-rapidity particles in the time projection chamber (TPC) and for spectator neutrons in the zero degree calorimeter (ZDC), respectively. Assuming that the CME is proportional to the magnetic field squared and the background is proportional to v_2 [67], one obtains

$$\begin{aligned}\Delta\gamma_{\text{CME}}(\psi_{\text{TPC}}) &= a\Delta\gamma_{\text{CME}}(\psi_{\text{ZDC}}), \\ \Delta\gamma_{\text{Bkg}}(\psi_{\text{ZDC}}) &= a\Delta\gamma_{\text{Bkg}}(\psi_{\text{TPC}}),\end{aligned}\quad (11)$$

where $a = \langle \cos [2(\psi_{\text{ZDC}} - \psi_{\text{TPC}})] \rangle$ and can be obtained from the v_2 measurement:

$$a = \frac{v_2(\psi_{\text{ZDC}})}{v_2(\psi_{\text{TPC}})}.\quad (12)$$

The CME signal relative to the inclusive $\Delta\gamma(\psi_{\text{TPC}})$ can be determined as

$$f_{\text{CME}} = \frac{\Delta\gamma_{\text{CME}}(\psi_{\text{TPC}})}{\Delta\gamma(\psi_{\text{TPC}})} = \frac{Aa - a^2}{1 - a^2}, \quad (13)$$

where A is defined as

$$A = \frac{\Delta\gamma(\psi_{\text{ZDC}})}{\Delta\gamma(\psi_{\text{TPC}})}. \quad (14)$$

It can be rewritten as

$$\begin{aligned} A &= f_{\text{CME}} \frac{(1/a)\Delta\gamma_{\text{CME}}(\psi_{\text{TPC}}) + a\Delta\gamma_{\text{Bkg}}(\psi_{\text{TPC}})}{\Delta\gamma_{\text{CME}}(\psi_{\text{TPC}})} \\ &= a + \left(\frac{1}{a} - a\right) f_{\text{CME}}, \end{aligned} \quad (15)$$

which one can solve for f_{CME} to obtain the last equality of (13). Note that A can also be measured experimentally. The left panel of Fig. 4 shows the STAR preliminary data on the centrality dependence of $\Delta\gamma$ with respect to the ZDC and TPC event planes in Au+Au collisions at 200 GeV and U+U collisions at 193 GeV. We see that $\Delta\gamma(\psi_{\text{ZDC}})$ is consistently lower than $\Delta\gamma(\psi_{\text{TPC}})$, which indicates that A is less than unity. This result indicates that the flow background contributes less to $\Delta\gamma(\psi_{\text{ZDC}})$ than to $\Delta\gamma(\psi_{\text{TPC}})$. Applying the above method, the STAR Collaboration extracted the CME fraction f_{CME} from different datasets for Au+Au collisions at 200 GeV and U+U collisions at 193 GeV; their results are summarized in the right panel of Fig. 4. The combined result for the CME fraction for Au+Au at 200 GeV and U+U at 193 GeV is $f_{\text{CME}} = 8 \pm 4 \pm 8\%$ [66]. Note that the CMS Collaboration has systematically measured different types of correlators γ_{ijk} in p+Pb collisions at 5.02 and 8.16 TeV and Pb+Pb collisions at 5.02 TeV, which provide constraints on the upper limit of the CME fraction, i.e., 13% for p+Pb and 7% for Pb+Pb collisions at the 95% confidence level [68, 69].

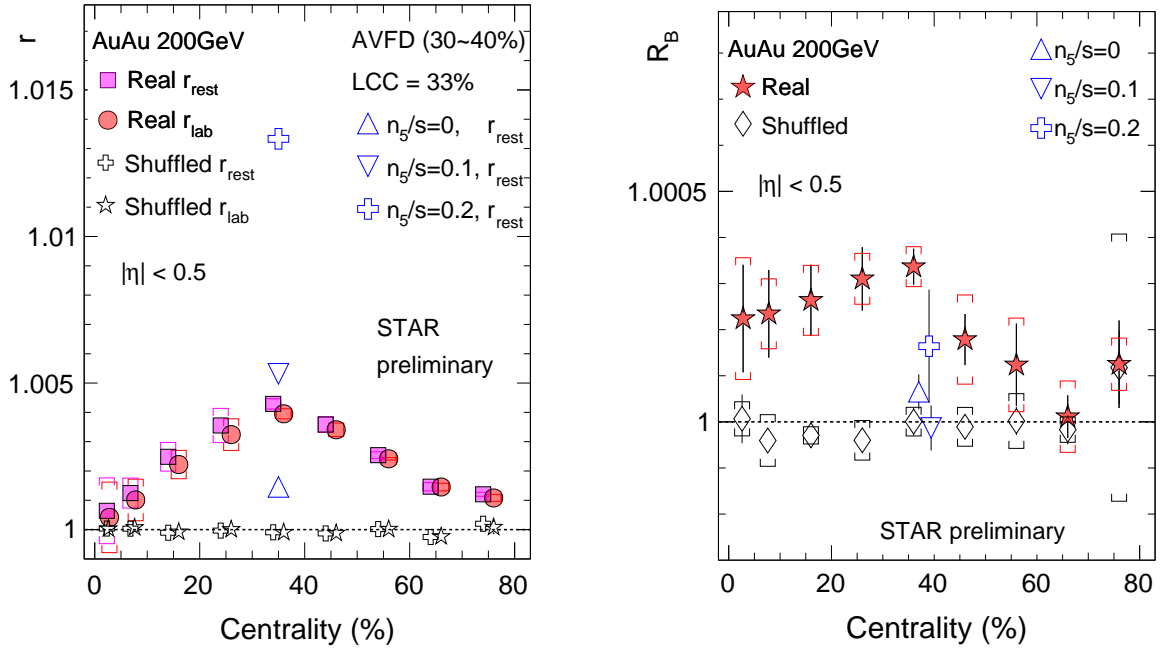


Fig. 5. STAR measurements of centrality dependence of r_{rest} , r_{lab} , and R_B from signed balance functions in Au+Au collisions at 200 GeV [70].

Many other methods of searching for the CME have been proposed, such as event shape engineering [69], the use of the H factor [71], and the invariant mass method [72]. See [11, 73] for recent reviews. A new observable, the signed balance function, was proposed recently; it is defined as [74]

$$B_{P,y}(S_y) = \frac{N_{+-}(S_y) - N_{++}(S_y)}{N_+} \quad (16)$$

and

$$B_{N,y}(S_y) = \frac{N_{-+}(S_y) - N_{--}(S_y)}{N_-}. \quad (17)$$

Note that $S_y = +1$ if particle α is leading particle β (i.e., $p_y^\alpha > p_y^\beta$), and $S_y = -1$ otherwise. $N_{+-}(S_y)$ denotes the number of positive–negative charge pairs with sign S_y in an event. $N_{++}(S_y)$, $N_{-+}(S_y)$, and $N_{--}(S_y)$ have similar definitions. $N_{+(-)}$ is the number of positive (negative) charge pairs in an event. Here the x axis is along the reaction plane, the z axis is along the beam direction, and the y axis is perpendicular to both the x and z axes. One can calculate an event using the event difference between B_P and B_N :

$$\delta B_y(\pm 1) = B_{P,y}(\pm 1) - B_{N,y}(\pm 1) \quad (18)$$

and

$$\Delta B_y = \delta B_y(+1) - \delta B_y(-1). \quad (19)$$

Note that ΔB_x can be defined similarly. When the CME is absent, for a positive–negative charge pair, the probability of the positive particle leading the negative one is equal to the probability of the opposite case. Thus, $B_{P,y(x)}$ and $B_{N,y(x)}$ measure the same quantity, in principle, and the distribution of $\Delta B_{y(x)}$ is subject only to statistical fluctuation. When the CME is present, the two probabilities become unbalanced within an event; thus, more pairs of particles of one charge type lead the other type. Therefore, for each event, $B_{P,y}$ and $B_{N,y}$ tend to differ; consequently, ΔB_y has a wider distribution. By contrast, the distribution of ΔB_x is not broadened, as there is no charge separation in the x direction. To cancel out the statistical fluctuation, one can define the ratio of the width of ΔB_y to that of ΔB_x as

$$r = \frac{\sigma_{\Delta B_y}}{\sigma_{\Delta B_x}} \quad (20)$$

to characterize the magnitude of the CME, because r will be greater than unity or unity with or without the CME, respectively. That is, the strength of the CME will be positively correlated with the deviation of r from unity. The ratio r can be calculated either in the laboratory frame (r_{lab}) or in the rest frame (r_{rest}) of the pair. One can take the ratio of these two cases:

$$R_B \equiv \frac{r_{\text{rest}}}{r_{\text{lab}}}, \quad (21)$$

where the subscript B indicates a balance function. It has been found that r_{lab} , r_{rest} , and R_B are sensitive not only to the strength of the CME, but also to the elliptic flow of primordial pions and ρ resonances, and even to the global spin alignment of the resonances [74]. Figure 5 presents the recent STAR measurement of the centrality dependence of r_{lab} , r_{rest} , and R_B from the signed balance functions in Au+Au collisions at 200 GeV [70]. In the 30–40% centrality bin, r_{rest} , r_{lab} , and R_B are all larger than the AVFD result without the CME and larger than unity, which supports the presence of the CME. However, none of the AVFD results for CMEs of different strengths can describe all three of these observables simultaneously. Therefore, more experimental and theoretical studies are needed.

Another new correlator, $R_{\Psi_2}(\Delta S) = C_{\Psi_2}(\Delta S)/C_{\Psi_2}^\perp(\Delta S)$, has been designed to measure the magnitude of the CME-induced charge separation parallel to the \vec{B} field [76, 77], where $C_{\Psi_2}(\Delta S)$ and $C_{\Psi_2}^\perp(\Delta S)$ are used to quantify the charge separation ΔS , i.e., the difference between the averaged $\langle \sin(\Delta\varphi_2) \rangle$ values of negatively and positively charged particles emitted about the estimated Ψ_2 plane, $\Delta\varphi_2 = \phi - \Psi_2$. Because the CME can result in charge separation along the \vec{B} field, one expects a concave $R_{\Psi_2}(\Delta S)$ distribution having a width that reflects the magnitude a_1 of the CME-induced charge separation. Because the reaction plane angle Ψ_2 is very weakly correlated with the \vec{B} field in small collision systems [78], the corresponding measurement in small systems can provide a baseline for the background contributions. The STAR Collaboration recently released the results for the R correlator [75]. Figure 6 compares the $R_{\Psi_2}(\Delta S'')$ correlators at $\langle N_{\text{ch}} \rangle \sim 20$ for p+Au, d+Au, and Au+Au collisions at 200 GeV. The convex or flat distributions shown for p(d)+Au collisions are consistent with the approximately random \vec{B} field relative to Ψ_2 expected in small collisions. By contrast, the Au+Au measurement relative to Ψ_2 shows a concave distribution, which is consistent with CME-driven charge separation according to the AVFD [76] and AMPT models [43, 44].

In addition to the CME, a gapless CMW could be formed by the interplay between the CME and CSE. The CMW results in an electric quadrupole moment in the initial coordinate space of the QGP [82, 83]. It can ultimately be transformed into a charge-asymmetry-dependent elliptic flow of pions by collective expansion [84]. Therefore, the elliptic flow of positively and negatively charged pions is given by

$$v_2(\pi^\pm) = v_2^{\text{base}} \mp \frac{r(\pi^\pm)}{2} A_{\text{ch}}, \quad (22)$$

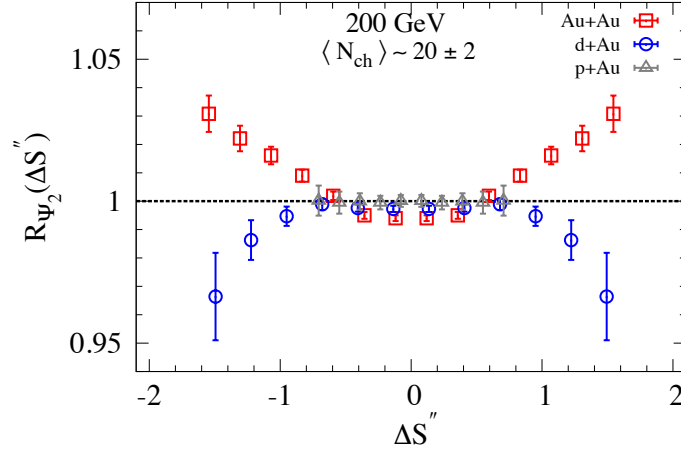


Fig. 6. STAR measurements of the $R_{\Psi_2}(\Delta S'')$ correlators obtained for charged particles in peripheral Au+Au and central $p(d)$ +Au collisions ($\langle N_{ch} \rangle \sim 20$) at 200 GeV, where $\Delta S''$ is the event-plane-resolution-corrected ΔS [75].

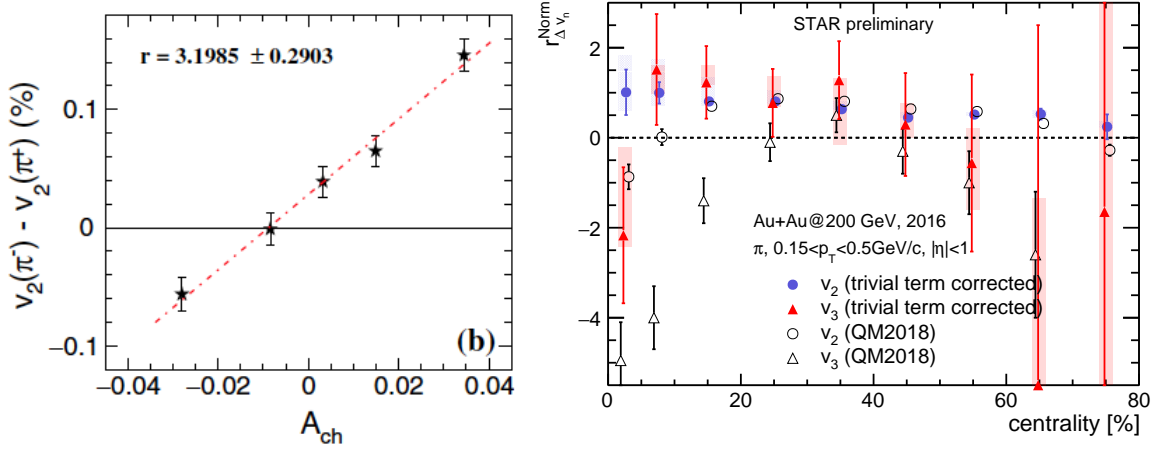


Fig. 7. STAR measurements of v_2 difference Δv_2 between π^- and π^+ as a function of charge asymmetry A_{ch} for Au+Au collisions at 200 GeV (30–40%) (left plot) [79]; centrality dependence of the slope parameter r of normalized $\Delta v_n(A_{ch})$ with and without trivial term correction in Au+Au collisions at 200 GeV [80, 81].

where

$$A_{ch} = \frac{N^+ - N^-}{N^+ + N^-} \quad (23)$$

is the charge asymmetry. The elliptic flow difference between positive and negative pions, $[\Delta v_2 = v_2(\pi^-) - v_2(\pi^+)]$, can then be fitted using the relation $\Delta v_2 = r A_{ch} + \Delta v_2(0)$. The left panel of Fig. 7 presents the results for Au+Au collisions at 200 GeV (30–40%) measured in the STAR experiment [79], where the slope parameter r is expected to reflect the strength of the CMW. In addition, because the third order of the event plane is not correlated with the magnetic field direction, measuring the slope parameter r from the triangular flow v_3 can provide a reference from the background in comparison with that from elliptic flow v_2 . However, care should be taken, because flow measurements by the Q-cumulant method using all the charged particles as a reference can introduce a trivial linear term to $\Delta v_n(A_{ch})$ owing to non-flow correlations. When all the charged

hadrons are used as reference particles, as is typically done in data analysis, the two-particle cumulant can be rewritten as [85]

$$d_n\{2; \pi^\pm h\} = \frac{d_n\{2; \pi^\pm h^+\} + d_n\{2; \pi^\pm h^-\}}{2} + \frac{d_n\{2; \pi^\pm h^+\} - d_n\{2; \pi^\pm h^-\}}{2} A_{\text{ch}}. \quad (24)$$

The second term on the right-hand side of (24) is proportional to A_{ch} and is opposite in sign for π^+ and π^- . These characteristics result directly in a trivial contribution to the CMW-sensitive slope parameter. Because non-flow correlations are always present in experimental data, the flow coefficients $d_n\{2; \text{pairs}\}$ from like-sign pairs and opposite-sign pairs differ. Therefore, the second term on the right-hand side of (24) is always finite as a trivial term, and it should be removed to detect the possible CMW signal. To eliminate the trivial linear A_{ch} term in practice, one can use hadrons of a single charge sign instead of all the charged hadrons as reference particles. One may use positive and negative particles separately as reference particles to obtain $v_n^\pi\{2; h^+\}$ and $v_n^\pi\{2; h^-\}$, and then take an average:

$$\bar{v}_n^\pi \equiv \frac{v_n^\pi\{2; h^+\} + v_n^\pi\{2; h^-\}}{2}. \quad (25)$$

Previous STAR results showed significant negative slopes for v_3 [86], which were thought to support the presence of the CMW. By applying the new method of removing the trivial term, the slope r can be corrected to some extent. As shown in the right-hand plot in Fig. 7, the normalized v_3 slopes are consistent with positive values (1.5σ above zero for 20–60% centrality), which are similar to the normalized v_2 slopes in terms of the relative magnitudes. In addition, it has been found that the non-flow correlations give rise to additional background in the slope of $\Delta v_n(A_{\text{ch}})$ owing to competition among different pion sources and the large multiplicity dilution of π^+ (π^-) at positive (negative) A_{ch} [80, 81]. Therefore, more detailed studies are needed to search for the CMW in the future.

III. QUANTUM KINETIC THEORY

In recent years, chiral kinetic theory (CKT) has been developed significantly [87–102] to describe various chiral effects in heavy-ion collisions. Numerical simulations based on the CKT have been developed [103–110]. However, with the discovery of global polarization at relatively low energies [5, 111], it is necessary to go beyond the chiral limit and develop a more general and practical quantum kinetic theory to describe spin effects for massive fermions. In this brief review, we consider only some of the works that were reported at the 2019 Quark Matter conference.

Most of these works are based on the Wigner functions but use slightly different realizations. The methods used in Refs. [112–114] are based on early works on the covariant Wigner functions [115–117]. The covariant Wigner function $W(x, p)$ for the Dirac fermion is defined as a two-point function:

$$W_{\alpha\beta}(x, p) = \int \frac{d^4 y}{(2\pi)^4} e^{-ip \cdot y} \left\langle \bar{\psi}_\beta \left(x + \frac{y}{2} \right) U \left(x + \frac{y}{2}, x - \frac{y}{2} \right) \psi_\alpha \left(x - \frac{y}{2} \right) \right\rangle, \quad (26)$$

where U denotes the gauge link along the straight line between $x - y/2$ and $x + y/2$. The Wigner function can generally be expanded as

$$W = \frac{1}{4} \left[\mathcal{F} + i\gamma^5 \mathcal{P} + \gamma^\mu \mathcal{V}_\mu + \gamma^5 \gamma^\mu \mathcal{A}_\mu + \frac{1}{2} \sigma^{\mu\nu} \mathcal{S}_{\mu\nu} \right], \quad (27)$$

where $\sigma^{\mu\nu} = (i/2)[\gamma^\mu, \gamma^\nu]$. One can choose the scalar function \mathcal{F} and axial vector function \mathcal{A}_μ as independent variables [112]; they are related to \mathcal{F} and \mathcal{A}_μ as

$$\mathcal{F} = \delta(p^2 - m^2) \mathcal{F} + \frac{\hbar}{m} \tilde{F}_{\mu\nu} p^\mu \mathcal{A}^\nu \delta'(p^2 - m^2), \quad (28)$$

$$\mathcal{A}_\mu = \delta(p^2 - m^2) \mathcal{A}_\mu + \frac{\hbar}{m} p^\nu \tilde{F}_{\mu\nu} \mathcal{F} \delta'(p^2 - m^2). \quad (29)$$

The kinetic equations for \mathcal{F} and \mathcal{A}_μ are given by

$$\begin{aligned} & p \cdot \nabla \left[\mathcal{F} \delta(p^2 - m^2) + \frac{\hbar}{m} \tilde{F}_{\mu\nu} p^\mu \mathcal{A}^\nu \delta'(p^2 - m^2) \right] \\ &= \frac{\hbar}{2m} (\partial_\lambda^x \tilde{F}_{\mu\nu}) \partial_p^\lambda [p^\mu \mathcal{A}^\nu \delta(p^2 - m^2)] \end{aligned} \quad (30)$$

and

$$\begin{aligned}
& p \cdot \nabla \left[\mathcal{A}_\mu \delta(p^2 - m^2) + \frac{\hbar}{m} p^\nu \tilde{F}_{\mu\nu} \mathcal{F} \delta'(p^2 - m^2) \right] \\
&= F_{\mu\nu} \left[\mathcal{A}^\nu \delta(p^2 - m^2) + \frac{\hbar}{m} p_\lambda \tilde{F}^{\nu\lambda} \mathcal{F} \delta'(p^2 - m^2) \right] \\
&+ \frac{\hbar}{2m} (\partial_\lambda^x \tilde{F}_{\mu\nu}) \partial_p^\lambda [p^\nu \mathcal{F} \delta(p^2 - m^2)], \tag{31}
\end{aligned}$$

together with the subsidiary condition $p \cdot \mathcal{A} \delta(p^2 - m^2) = 0$, where $\nabla^\mu = \partial_x^\mu - F^{\mu\nu} \partial_\nu^p$, and $\tilde{F}_{\mu\nu} = \epsilon_{\mu\nu\rho\sigma} F^{\rho\sigma} / 2$. The integrated kinetic equation in three-vector form can be obtained by integrating the zero component of the momentum:

$$(\nabla_t + \mathbf{v} \cdot \nabla) \mathcal{F} = -\frac{\hbar}{2mE_p} \left[(\mathbf{B} + \mathbf{E} \times \mathbf{v})(\mathbf{v} \cdot \nabla + E_p \overleftarrow{\nabla}_x \cdot \nabla_p) - (\mathbf{B} \cdot \mathbf{v})(\mathbf{v} \cdot \nabla + E_p \overleftarrow{\nabla}_x \cdot \nabla_p \mathbf{v}) \right] \cdot \vec{\mathcal{A}}, \tag{32}$$

$$(\nabla_t + \mathbf{v} \cdot \nabla) \vec{\mathcal{A}} = \mathbf{B} \times \vec{\mathcal{A}} - \mathbf{E}(\mathbf{v} \cdot \vec{\mathcal{A}}) - \frac{\hbar}{2mE_p} (\mathbf{B} + \mathbf{E} \times \mathbf{v})(\mathbf{v} \cdot \nabla + E_p \overleftarrow{\nabla}_x \cdot \nabla_p) \mathcal{F}, \tag{33}$$

where $\mathbf{v} = \mathbf{p}/E_p$, $E_p = \sqrt{\mathbf{p}^2 + m^2}$, $\nabla_t = \partial_t + \mathbf{E} \cdot \nabla_p$, $\nabla = \nabla_x + \mathbf{B} \times \nabla_p$, and the left arrow over ∇_x denotes that it acts only on the electromagnetic fields on its left. When this method is used, various spin effects such as the chiral anomaly, CSE, quantum magnetization effect, and global polarization effect emerge naturally. It can be shown that the Dirac sea or vacuum contribution originating from the anti-commutation relations between antiparticle field operators in the Wigner function without a normal-order operator plays a crucial role in generating the chiral anomaly in quantum kinetic theory for both massive and massless fermions [118]. The coefficient of the chiral anomaly derived in this way is universal and is independent of the phase space distribution function at zero momentum.

Weickgenannt *et al.* [113, 114] also derived the kinetic theory for massive spin-1/2 particles in the covariant Wigner function formalism. They chose the scalar and tensor components, \mathcal{F} and $\mathcal{S}_{\mu\nu}$, as the basis from which the other components can be derived; these components are related to the distribution function V and tensor distribution or dipole moment $\bar{\Sigma}_{\mu\nu}$ as independent variables of $O(\hbar)$:

$$\mathcal{F} = \delta(p^2 - m^2) mV - \frac{\hbar}{2} m F_{\mu\nu} \bar{\Sigma}^{\mu\nu} \delta'(p^2 - m^2), \tag{34}$$

$$\mathcal{S}_{\mu\nu} = \delta(p^2 - m^2) m \bar{\Sigma}_{\mu\nu} - \hbar F_{\mu\nu} V \delta'(p^2 - m^2), \tag{35}$$

where $\delta'(x) \equiv d\delta(x)/dx$, $V = V_{(0)} + \hbar V_{(1)}$, and $\bar{\Sigma}^{\mu\nu} = \Sigma_{(0)}^{\mu\nu} A_{(0)} + \hbar \Sigma_{(1)}^{\mu\nu}$. In addition, $V_{(0)}$ and $A_{(0)}$ are scalar functions of the phase space and can be expressed as particle number distributions [113, 114]. The kinetic equations for these functions are given by

$$\begin{aligned}
0 &= \delta(p^2 - m^2) \left[p \cdot \nabla V + \frac{\hbar}{4} (\partial_x^\alpha F^{\mu\nu}) \partial_p^\alpha \bar{\Sigma}_{\mu\nu} \right] \\
&- \frac{\hbar}{2} \delta'(p^2 - m^2) F^{\alpha\beta} p \cdot \nabla \bar{\Sigma}_{\alpha\beta} \\
0 &= \delta(p^2 - m^2) \left[p \cdot \nabla \bar{\Sigma}_{\mu\nu} - F_{[\mu}^{\alpha} \bar{\Sigma}_{\nu]\alpha} + \frac{\hbar}{2} (\partial_x^\alpha F_{\mu\nu}) \partial_p^\alpha V \right] \\
&- \hbar \delta'(p^2 - m^2) F_{\mu\nu} p \cdot \nabla V. \tag{36}
\end{aligned}$$

together with one constraint equation, $p^\nu \bar{\Sigma}_{\mu\nu} \delta(p^2 - m^2) = \hbar \delta(p^2 - m^2) \nabla_\mu^V / 2$. In this method, the kinetic equations and the components of the Wigner function are invariant under the transformation

$$\begin{aligned}
\bar{\Sigma}_{\mu\nu} &\rightarrow \hat{\bar{\Sigma}}_{\mu\nu} = \bar{\Sigma}_{\mu\nu} + (p^2 - m^2) \delta \bar{\Sigma}_{\mu\nu}, \\
V &\rightarrow \hat{V} = V - \frac{\hbar}{2} F^{\mu\nu} \delta \bar{\Sigma}_{\mu\nu}, \tag{37}
\end{aligned}$$

or the transformation

$$\begin{aligned}
V &\rightarrow \hat{V} = V + (p^2 - m^2) \delta V, \\
\bar{\Sigma}_{\mu\nu} &\rightarrow \hat{\bar{\Sigma}}_{\mu\nu} = \bar{\Sigma}_{\mu\nu} - \hbar F_{\mu\nu} \delta V, \tag{38}
\end{aligned}$$

where δV and $\delta\bar{\Sigma}_{\mu\nu}$ are arbitrary functions of x and p that are nonsingular on the mass shell. When these transformations are used, the derivative terms of the delta function can be omitted from the kinetic equations, greatly reducing the results. Agreement with the CKT has been obtained by replacing the dipole-moment tensor $\bar{\Sigma}_{\mu\nu}$ with its counterpart in the massless case. The kinetic equations yield a special single-particle distribution in global equilibrium with rigid rotation. When this distribution is used, analogs of various spin effects appear, such as the CME and CSE, for massive fermions. A smooth connection between the kinetic theory of massive spin-1/2 particles and the CKT was found recently [119] by introducing a frame-dependent decomposition of the dipole-moment tensor $\bar{\Sigma}_{\mu\nu}$.

All the components of the covariant Wigner function can be derived from \mathcal{V}^μ and \mathcal{A}^μ for massive fermions in the Schwinger–Keldysh formalism [120]. The CKT for the massless case can be recovered from the formula for massive fermions. The kinetic equation has been generalized to include collision terms in the Schwinger–Keldysh formalism [121].

A covariant kinetic equation for massive fermions in curved spacetime and an external electromagnetic field can also be derived. Liu et al. [122] use a general covariant Wigner function formalism not only under the $U(1)$ gauge and local Lorentz transformation but also under diffeomorphism, which is compatible with general relativity. The spin polarization in the presence of Riemann curvature and an electromagnetic field in both local and global equilibrium has also been studied.

Integration of the covariant Wigner function over p_0 yields the equal-time Wigner function [123–125]. Compared to the covariant form, the equal-time form loses obvious Lorentz covariance, but it is more convenient for time evolution problems such as pair production in a strong electric field [126, 127]. The kinetic equation can also be derived from the equal-time Wigner functions. The equal-time Wigner function $\mathcal{W}(x, \mathbf{p})$ can be obtained from the covariant one $W(x, p)$:

$$\mathcal{W}(x, \mathbf{p}) = \int dp_0 W(x, p) \gamma^0. \quad (39)$$

It can be decomposed into the following components:

$$\begin{aligned} \mathcal{W} = \frac{1}{4} [& f_0 + \gamma_5 f_1 - i\gamma_0 \gamma_5 f_2 + \gamma_0 f_3 + \gamma_5 \gamma_0 \boldsymbol{\gamma} \cdot \mathbf{g}_0 \\ & + \gamma_0 \boldsymbol{\gamma} \cdot \mathbf{g}_1 - i\boldsymbol{\gamma} \cdot \mathbf{g}_2 - \gamma_5 \boldsymbol{\gamma} \cdot \mathbf{g}_3]. \end{aligned} \quad (40)$$

The fermion number density f_0 and spin current \mathbf{g}_0 are chosen to be independent components; their kinetic equations are derived as [128]

$$\left(\nabla_t \pm \frac{\mathbf{p}}{E_p} \cdot \nabla \right) f_0^\pm = \frac{\hbar \mathbf{E}}{2E_p^2} \cdot \nabla \times \mathbf{g}_0^\pm \mp \frac{\hbar}{2E_p^3} \mathbf{B} \cdot (\mathbf{p} \cdot \nabla) \mathbf{g}_0^\pm + \frac{\hbar \mathbf{B} \times \mathbf{p}}{E_p^4} \cdot \mathbf{E} \times \mathbf{g}_0^\pm, \quad (41)$$

$$\begin{aligned} \left(\nabla_t \pm \frac{\mathbf{p}}{E_p} \cdot \nabla \right) \mathbf{g}_0^\pm = \frac{1}{E_p^2} [& \mathbf{p} \times (\mathbf{E} \times \mathbf{g}_0^\pm) \mp E_p \mathbf{B} \times \mathbf{g}_0^\pm] \mp \hbar \left(\frac{\mathbf{B}}{2E_p^3} \pm \frac{\mathbf{E} \times \mathbf{p}}{2E_p^4} \right) \mathbf{p} \cdot \nabla f_0^\pm \\ & \mp \hbar \left(\frac{(\mathbf{p} \cdot \mathbf{E})(\mathbf{E} \times \mathbf{p})}{E_p^5} \pm \frac{\mathbf{p} \times (\mathbf{B} \times \mathbf{E})}{2E_p^4} \right) f_0^\pm. \end{aligned} \quad (42)$$

where the superscripts $+$ and $-$ indicate the particle and antiparticle, respectively. The small mass expansion can be performed. The mass correction changes only the structure of the chiral kinetic equation in terms of the effective collision terms, which is only a first-order quantum correction to the CME.

All the works mentioned above are valid only up to the first order of \hbar and without collision terms for particle scattering. In addition to these works based on Wigner functions, Li and Yee [129] derived the kinetic equations for the spin-density matrix in the Schwinger–Keldysh formalism. Specifically, they formulated collision terms for fermions from their interactions with the QGP medium. However, they consider only the spatial homogeneity limit; thus, the collisions are local and do not involve the vorticity. The time evolution equations are derived for the particle number distribution $f(\mathbf{p}, t)$ and the spin polarization density $\mathbf{S}(\mathbf{p}, t)$ in the leading log order of $g^4 \log(1/g)$:

$$\begin{aligned} \frac{\partial f(\mathbf{p}, t)}{\partial t} &= C_2(F) \frac{m_D^2 g^2 \log(1/g)}{(4\pi)} \cdot \frac{1}{2pE_p} \Gamma_f, \\ \frac{\partial \mathbf{S}(\mathbf{p}, t)}{\partial t} &= C_2(F) \frac{m_D^2 g^2 \log(1/g)}{(4\pi)} \cdot \frac{1}{2pE_p} \Gamma_S, \end{aligned} \quad (43)$$

where $C_2(F) = (N_c^2 - 1)/2N_c$, and Γ_f and Γ_S are diffusion-like differential operators in momentum space that contain up to the second-order derivatives of the momentum. The explicit forms of Γ_f and Γ_S are given in Eq. (4.70) of Ref. [129].

Note that the quantum kinetic equation for massive fermions is very different from the chiral kinetic equation for massless fermions. The kinetic equation for massive fermions includes four coupled independent functions; one of them gives the particle distribution function, and the other three give the spin polarization vector. By contrast, the kinetic equation for massless fermions contains only one distribution function. The reason is that the spin direction coincides with the momentum of the

fermion and is not a dynamical quantity at the chiral limit; however, for the massive case, the spin does not coincide with the momentum and becomes dynamical. It was thought that the chiral kinetic equation could be obtained from the quantum kinetic equation for massive fermions by naively taking the massless limit; however, this limit was found to be more important than it appears. The most recent works on this problem can be found in Refs. [119, 130].

IV. SPIN POLARIZATION EFFECTS

A. Theoretical progress

In early works [131, 132], Liang and Wang proposed that particles can be polarized as a result of the global OAM in non-central heavy-ion collisions. The formation of the vorticity in heavy-ion collisions was subsequently studied [133]. Becattini and his collaborators [134–136] performed a systematic study of statistical models of relativistic spinning particles. In addition, recent review articles are cited in Refs. [137–139].

The initial global OAM is estimated to be as large as $J_0 \sim 10^5 \hbar$ in 200 GeV Au+Au collisions with the impact parameter $b = 10$ fm. Consequently, the QGP is found to be the most vortical fluid ever observed in nature. The vorticity properties can be studied using the AMPT and HIJING [140–142], UrQMD [143], and hydrodynamic models [144–149]. The vorticity is found to be more strongly suppressed at higher collision energies. One can find further discussion in Refs. [150–152] and reference therein.

The spin polarization per particle for spin-1/2 fermions with momentum p at freeze-out can be derived using the statistical model for relativistic spinning particles [136] and the Wigner functions [153]:

$$S^\mu(p) = -\frac{1}{8m} \frac{\epsilon^{\mu\nu\rho\sigma} p_\nu \int d\Sigma_\lambda p^\lambda (u \cdot p)^{-1} f_{\text{FD}}(1 - f_{\text{FD}}) \omega_{\rho\sigma}^{\text{th}}(x)}{\int d\Sigma_\lambda p^\lambda f_{\text{FD}}}, \quad (44)$$

where Σ_λ denotes the freeze-out hypersurface, S^μ is the Pauli–Lubanski pseudo-vector, m is the fermion mass, $f_{\text{FD}} \equiv f_{\text{FD}}(x, \mathbf{p})$ is the Fermi–Dirac distribution. In addition,

$$\omega_{\rho\sigma}^{\text{th}} = \frac{1}{2} (\partial_\sigma \beta_\rho - \partial_\rho \beta_\sigma) \quad (45)$$

is the thermal vorticity, where u^μ is the fluid velocity, and $\beta_\rho = u_\rho/T$ is the temperature four-vector. Equation (44) has been widely used in hydrodynamics models and transport models to calculate the spin polarization of hyperons.

In quantum field theory, the decomposition of the total angular momentum into the orbital and spin components for massive particles with spin is not unique. Different decompositions are related by a pseudo-gauge transformation. Although the energy-momentum tensor $\hat{T}^{\mu\nu}$ and spin tensor $\hat{S}^{\lambda;\mu\nu}$ depend on the decomposition, the total energy-momentum and total angular momentum are invariant under the pseudo-gauge transformation. A special pseudo-gauge transformation is the transformation of the canonical definitions of $\hat{T}_C^{\mu\nu}$ and $\hat{S}_C^{\lambda;\mu\nu}$ into the Belinfante $\hat{T}_B^{\mu\nu}$, which absorbs $\hat{S}_C^{\lambda;\mu\nu}$; i.e., $\hat{S}_B^{\lambda;\mu\nu} = 0$. Thus, the total angular momentum consists only of the orbital component. The Belinfante energy-momentum tensor is symmetric with respect to its two indices: $\hat{T}_B^{\mu\nu} = \hat{T}_B^{\nu\mu}$.

The thermal properties of a quantum field system can be described by the density operator $\hat{\rho}$. The density operator in local equilibrium can be determined from the maximal entropy principle [154–156] under given densities of conserved currents on the space-like hypersurface Σ . This is done by maximizing $S = -\text{Tr}(\hat{\rho} \log \hat{\rho})$ under the conditions

$$\begin{aligned} n_\mu \text{Tr} \left(\hat{\rho} \hat{T}^{\mu\nu} \right) &= n_\mu T^{\mu\nu}, \\ n_\mu \text{Tr} \left(\hat{\rho} \hat{j}^\mu \right) &= n_\mu j^\mu, \end{aligned} \quad (46)$$

where n_μ is the normal vector of Σ . The constraint on the total angular momentum density can generally be included as well:

$$\begin{aligned} n_\lambda \text{Tr} \left(\hat{\rho} \hat{\mathcal{J}}^{\lambda;\mu\nu} \right) &= n_\lambda \text{Tr} \left[\hat{\rho} \left(x^\mu \hat{T}^{\lambda\nu} - x^\nu \hat{T}^{\lambda\mu} + \hat{S}^{\lambda;\mu\nu} \right) \right] \\ &= n_\lambda \mathcal{J}^{\lambda;\mu\nu}. \end{aligned} \quad (47)$$

For the Belinfante energy-momentum tensor, however, the above condition is automatically satisfied by using (46). In this case, the density operator at local equilibrium has the form

$$\hat{\rho}_{\text{LE}} = \frac{1}{Z} \exp \left[- \int_\Sigma d\Sigma_\mu \left(\hat{T}_B^{\mu\nu} \beta_\nu - \zeta \hat{j}^\mu \right) \right], \quad (48)$$

where β^ν and ζ are the Lagrange multiplier functions of space-time; the former is the temperature four-vector, and the latter is the ratio of the chemical potential to the temperature [156].

In general, $\hat{\rho}_{\text{LE}}$ in (48) depends on the time τ as $\Sigma_\mu(\tau)$. One can rewrite the exponent of $\hat{\rho}_{\text{LE}}$ as

$$\begin{aligned} & \int_{\Sigma(\tau)} d\Sigma_\mu \left(\hat{T}_B^{\mu\nu} \beta_\nu - \zeta \hat{j}^\mu \right) \\ &= \int_{\Sigma(\tau_0)} d\Sigma_\mu \left(\hat{T}_B^{\mu\nu} \beta_\nu - \zeta \hat{j}^\mu \right) \\ & - \int_{\Theta} d\Theta \left(\hat{T}_B^{\mu\nu} \partial_\mu \beta_\nu - \hat{j}^\mu \partial_\mu \zeta \right), \end{aligned} \quad (49)$$

where Θ is the space-time volume bounded by $\Sigma(\tau)$, $\Sigma(\tau_0)$, and the time-like boundary connecting $\Sigma(\tau)$ and $\Sigma(\tau_0)$. Here we used

$$\partial_\mu \left(\hat{T}_B^{\mu\nu} \beta_\nu - \zeta \hat{j}^\mu \right) = \hat{T}_B^{\mu\nu} \partial_\mu \beta_\nu - \hat{j}^\mu \partial_\mu \zeta, \quad (50)$$

where we used the conservation of energy-momentum and current. To make $\hat{\rho}_{\text{LE}}$ independent of the choice of $\Sigma_\mu(\tau)$, i.e., to obtain the global equilibrium density matrix $\hat{\rho}_{\text{GE}}$, the following conditions must be met:

$$\begin{aligned} \partial_\mu \beta_\nu + \partial_\nu \beta_\mu &= 0, \\ \partial_\mu \zeta &= 0, \end{aligned} \quad (51)$$

according to which ζ is constant and β^μ is a Killing vector:

$$\beta^\mu = \omega_{\text{th}}^{\mu\nu} x_\nu + b^\mu, \quad (52)$$

where $\omega_{\text{th}}^{\mu\nu}$ is a constant antisymmetric tensor given by (45), and b^μ is a constant vector. The local equilibrium density operator in (48) can be expressed in terms of the canonical energy-momentum and spin tensors:

$$\begin{aligned} \hat{\rho}_{\text{LE}} &= \frac{1}{Z} \exp \left\{ - \int_{\Sigma} d\Sigma_\mu \left[\hat{T}_C^{\mu\nu} \beta_\nu - \zeta \hat{j}^\mu - \frac{1}{2} \omega_{\lambda\nu}^{\text{th}} \hat{S}_C^{\mu;\lambda\nu} \right. \right. \\ & \left. \left. - \frac{1}{2} (\partial_\lambda \beta_\nu + \partial_\nu \beta_\lambda) \left(\hat{S}_C^{\lambda;\mu\nu} + \hat{S}_C^{\nu;\mu\lambda} \right) \right] \right\}. \end{aligned} \quad (53)$$

If we substitute (51) and (52) in the above expression for $\hat{\rho}_{\text{LE}}$, we obtain $\hat{\rho}_{\text{GE}}$:

$$\hat{\rho}_{\text{GE}} = \frac{1}{Z} \exp \left[-b_\mu \hat{P}^\mu + \frac{1}{2} \omega_{\lambda\nu}^{\text{th}} \hat{J}^{\lambda\nu} + \zeta \hat{Q} \right], \quad (54)$$

where \hat{P}^μ , $\hat{J}^{\lambda\nu}$, and \hat{Q} are given by

$$\begin{aligned} \hat{P}^\nu &= \int_{\Sigma} d\Sigma_\mu \hat{T}^{\mu\nu}, \\ \hat{J}^{\lambda\nu} &= \int_{\Sigma} d\Sigma_\mu \mathcal{J}^{\mu;\lambda\nu}, \\ \hat{Q} &= \int_{\Sigma} d\Sigma_\mu \hat{j}^\mu. \end{aligned} \quad (55)$$

If we work with the canonical energy-momentum and spin tensors, we have to impose the constraint in (47), which also constrains the spin tensor:

$$n_\lambda \text{Tr} \left(\hat{\rho} \hat{S}_C^{\lambda;\mu\nu} \right) = n_\lambda S_C^{\lambda;\mu\nu}. \quad (56)$$

This introduces a spin chemical potential, the antisymmetric tensor $\Omega_{\lambda\nu}$, as a Lagrange multiplier into the equation for $\hat{\rho}_{\text{LE}}$:

$$\hat{\rho}_{\text{LE}} = \frac{1}{Z} \exp \left[- \int_{\Sigma} d\Sigma_\mu \left(\hat{T}_C^{\mu\nu} \beta_\nu - \frac{1}{2} \Omega_{\lambda\nu} \hat{S}_C^{\mu;\lambda\nu} - \zeta \hat{j}^\mu \right) \right]. \quad (57)$$

Comparing (57) with (53), we see that $\hat{\rho}_{\text{LE}}$ is the same for the Belinfante and canonical tensors under the following conditions:

(a) the field β^μ is the same in both cases; (b) $\Omega_{\lambda\nu} = \omega_{\lambda\nu}^{\text{th}}$; and (c) $(\partial_\lambda \beta_\nu + \partial_\nu \beta_\lambda) \left(\hat{S}_C^{\lambda;\mu\nu} + \hat{S}_C^{\nu;\mu\lambda} \right) = 0$. We can see that

if $\Omega_{\lambda\nu} = \omega_{\lambda\nu}^{\text{th}}$ and $\partial_\lambda\beta_\nu + \partial_\nu\beta_\lambda = 0$, then $\hat{\rho}_{\text{LE}}$ for the canonical tensors becomes the same as $\hat{\rho}_{\text{GE}}$ for the Belinfante tensor in (54). Therefore, one can conclude that the density operator in global equilibrium is pseudo-gauge-invariant, but in local equilibrium, it depends on the pseudo-gauge [157].

If we choose the Belinfante tensors or $\hat{\rho}_{\text{LE}}$ in (48) or (53), the spin relaxation time is microscopically small, and the value of the spin potential agrees with the thermal vorticity almost immediately. If we choose the canonical tensors or $\hat{\rho}_{\text{LE}}$ in (57) with the spin chemical potential, the spin density slowly reaches global equilibrium, just as a conserved charge density or energy density does, and finally the spin chemical potential should converge to the thermal vorticity [157].

Similar problems involving the decomposition of the total angular momentum of quarks and gluons in the proton spin (see Ref. [158] for a review) have been widely debated in the QCD community for years. Two well-known decomposition methods are that of Jaffe and Manohar and that of Ji, which are close to the canonical and Belinfante tensor forms, respectively. A review article [159] discusses the difference between the Belinfante and canonical forms. For a chiral medium, the decomposition can be found in Ref. [160].

If we choose a specific pseudo-gauge, for example, the canonical form that has the spin tensor, the spin chemical potential $\Omega_{\lambda\nu}$ must be introduced into $\hat{\rho}_{\text{LE}}$, as shown in (57). Therefore, we have another conservation equation in addition to the conservation of energy-momentum and charge:

$$\partial_\mu j^\mu = 0, \quad \partial_\mu T^{\mu\nu} = 0, \quad \partial_\lambda S^{\lambda,\mu\nu} = T^{\nu\mu} - T^{\mu\nu}, \quad (58)$$

where the energy-momentum tensor, charge current, and spin tensor can be obtained through $\hat{\rho}_{\text{LE}}$:

$$\begin{aligned} T^{\mu\nu} &= \text{tr} \left(\hat{\rho}_{\text{LE}} \hat{T}^{\mu\nu} \right), \\ j^\mu &= \text{tr} \left(\hat{\rho}_{\text{LE}} \hat{j}^\mu \right), \\ S^{\mu,\nu\lambda} &= \text{tr} \left(\hat{\rho}_{\text{LE}} \hat{S}^{\mu,\nu\lambda} \right). \end{aligned} \quad (59)$$

All the above quantities are functions of β^μ , ζ , and $\Omega_{\lambda\nu}$. There are a total of 11 independent equations and variables. These equations make up a full set of hydrodynamic equations including the spin degrees of freedom. There have been a few attempts in spin hydrodynamics [37, 157, 161–165]. Another approach using Lagrangian techniques can also provide some information about the local equilibrium [166–169].

Spin degrees of freedom can be introduced into the phase space distribution for spin-1/2 fermions by generalizing the scalar function to a 2×2 Hermitian matrix [136]:

$$\begin{aligned} f_{rs}^+(x, p) &= \frac{1}{2m} \bar{u}_r(p) X^+ u_s(p), \\ f_{rs}^-(x, p) &= -\frac{1}{2m} \bar{v}_r(p) X^- v_s(p), \end{aligned} \quad (60)$$

where $r, s = \pm 1$; u_r and v_r are Dirac spinors normalized by $\bar{u}_r(p)u_s(p) = 2m\delta_{rs}$ and $\bar{v}_r(p)v_s(p) = -2m\delta_{rs}$, respectively; and X^\pm are 4×4 matrices defined as

$$X^\pm = \exp \left(-\beta_\mu p^\mu \pm \zeta \pm \frac{1}{4} \Omega_{\mu\nu} \sigma^{\mu\nu} \right). \quad (61)$$

The Wigner functions in equilibrium for fermions and antifermions are given by

$$\begin{aligned} W_{\text{eq}}^+(x, k) &= \sum_{r,s} \int d^4p \theta(p_0) \delta(p^2 - m^2) \delta^{(4)}(k-p) u_r(p) \bar{u}_s(p) f_{rs}^+(x, p) \\ &= \frac{1}{2m} \int d^4p \theta(p_0) \delta(p^2 - m^2) \delta^{(4)}(k-p) (p_\mu \gamma^\mu + m) X^+ (p_\mu \gamma^\mu + m), \\ W_{\text{eq}}^-(x, k) &= -\sum_{r,s} \int d^4p \theta(-p_0) \delta(p^2 - m^2) \delta^{(4)}(k+p) v_r(p) \bar{v}_s(p) f_{rs}^-(x, p) \\ &= \frac{1}{2m} \int d^4p \theta(-p_0) \delta(p^2 - m^2) \delta^{(4)}(k-p) (p_\mu \gamma^\mu - m) X^- (p_\mu \gamma^\mu - m). \end{aligned} \quad (62)$$

The total Wigner function is the sum of them:

$$W_{\text{eq}}(x, k) = W_{\text{eq}}^+(x, k) + W_{\text{eq}}^-(x, k). \quad (63)$$

The components of $W_{\text{eq}}(x, k)$ are given in (27) and can be extracted by taking the traces of $\Gamma_i W_{\text{eq}}(x, k)$ with $\Gamma_i = 1, \gamma^5, \gamma^\mu, \gamma^5 \gamma^\mu, \sigma^{\mu\nu}$.

The energy-momentum and spin tensors proposed by de Groot, van Leeuwen, and van Weert (GLW) [170] can be extracted from the Wigner function [163]:

$$\begin{aligned} T_{\text{GLW}}^{\mu\nu} &= \frac{1}{m} \int d^4k k^\mu k^\nu \mathcal{F}, \\ S_{\text{GLW}}^{\lambda;\mu\nu} &= \frac{1}{4} \int d^4k \text{Tr} \left[\{ \sigma^{\mu\nu}, \gamma^\lambda \} W + \frac{2i}{m} \left(\gamma^{[\mu} k^{\nu]} \gamma^\lambda - \gamma^\lambda \gamma^{[\mu} k^{\nu]} \right) W \right]. \end{aligned} \quad (64)$$

In equilibrium, we use $W = W_{\text{eq}}$ in (63) and obtain $T_{\text{GLW}}^{\mu\nu} = T_{\text{eq}}^{\mu\nu}$ and $S_{\text{GLW}}^{\lambda;\mu\nu} = S_{\text{eq}}^{\lambda;\mu\nu}$. Because the GLW energy-momentum tensor is symmetric, the GLW spin tensor should be conserved separately. Thus, the conservation laws read

$$\partial_\mu j^\mu = 0, \quad \partial_\mu T_{\text{GLW}}^{\mu\nu} = 0, \quad \partial_\lambda S_{\text{GLW}}^{\lambda;\mu\nu} = 0. \quad (65)$$

The canonical forms of the energy-momentum and spin tensors can be obtained from the Dirac Lagrangian [113, 117]:

$$\begin{aligned} T_C^{\mu\nu} &= \int d^4k k^\nu \mathcal{V}^\mu, \\ S_C^{\lambda;\mu\nu} &= \frac{1}{4} \int d^4k \text{Tr} [\{ \sigma^{\mu\nu}, \gamma^\lambda \} W] = -\frac{1}{2} \epsilon^{\lambda\mu\nu\rho} \int d^4k \mathcal{A}_\rho. \end{aligned} \quad (66)$$

One can verify that the canonical tensor forms are related to the GLW forms by the pseudo-gauge transformation [163]. The explicit relation between the two tensor forms can be written as

$$\begin{aligned} T_C^{\mu\nu} &= T_{\text{GLW}}^{\mu\nu} - \frac{\hbar}{2m} \int d^4k k^\nu \partial_\lambda S_{\text{eq}}^{\lambda\mu} = T_{\text{GLW}}^{\mu\nu} - \partial_\lambda S_{\text{GLW}}^{\nu;\lambda\mu}, \\ S_C^{\lambda;\mu\nu} &= S_{\text{GLW}}^{\lambda;\mu\nu} + S_{\text{GLW}}^{\mu;\nu\lambda} + S_{\text{GLW}}^{\nu;\lambda\mu}. \end{aligned} \quad (67)$$

One can verify that the conservation laws for $T_C^{\mu\nu}$ and $S_C^{\lambda;\mu\nu}$ follow those for $T_{\text{GLW}}^{\mu\nu}$ and $S_{\text{GLW}}^{\lambda;\mu\nu}$ in (65).

However, it is still an open question whether the QGP reaches a local equilibrium of the spin degrees of freedom. A microscopic model of the spin polarization generated by spin-orbit coupling in particle collisions has been proposed [171]. Without assuming a local equilibrium of spins, it uses an effective method of wave packets to handle particle scattering for specified impact parameters. The spin-vorticity coupling naturally emerges from the spin-orbit coupling encoded in the polarized scattering amplitudes of collisional integrals when a local equilibrium of the momentum is assumed. First, the collision rate is calculated:

$$R_{AB \rightarrow 12} = n_A n_B |v_A - v_B| \sigma = \frac{d^3 p_A}{(2\pi)^3} \frac{d^3 p_B}{(2\pi)^3} f_A(x_A, p_A) f_B(x_B, p_B) |v_A - v_B| \Delta\sigma, \quad (68)$$

where $v_A = |\mathbf{p}_A|/E_A$ and $v_B = -|\mathbf{p}_B|/E_B$ are the longitudinal velocities, with $\mathbf{p}_A = -\mathbf{p}_B$ in the center-of-mass frame of colliding particles; f_A and f_B are the phase space distributions of the incident particles A and B , respectively; and $\Delta\sigma$ denotes the infinitesimal element of the cross section. After incorporating the components of the wave packets, the matrix elements of 2-to-2 scattering, the spin projection, and the proper Lorentz transformations, one obtains the polarization production rate per unit volume:

$$\begin{aligned} \frac{d^4 \mathbf{P}_{AB \rightarrow 12}(X)}{dX^4} &= \frac{1}{(2\pi)^4} \int \frac{d^3 p_{c,A}}{(2\pi)^3 2E_{c,A}} \frac{d^3 p_{c,B}}{(2\pi)^3 2E_{c,B}} \frac{d^3 p_{c,1}}{(2\pi)^3 2E_{c,1}} \frac{d^3 p_{c,2}}{(2\pi)^3 2E_{c,2}} \\ &\quad \times |v_{c,A} - v_{c,B}| G_1 G_2 \int d^3 k_{c,A} d^3 k_{c,B} d^3 k'_{c,A} d^3 k'_{c,B} \\ &\quad \times \phi_A(\mathbf{k}_{c,A} - \mathbf{p}_{c,A}) \phi_B(\mathbf{k}_{c,B} - \mathbf{p}_{c,B}) \phi_A^*(\mathbf{k}'_{c,A} - \mathbf{p}_{c,A}) \phi_B^*(\mathbf{k}'_{c,B} - \mathbf{p}_{c,B}) \\ &\quad \times \delta^{(4)}(k'_{c,A} + k'_{c,B} - p_{c,1} - p_{c,2}) \delta^{(4)}(k_{c,A} + k_{c,B} - p_{c,1} - p_{c,2}) \\ &\quad \times \int d^2 \mathbf{b}_c f_A \left(X_c + \frac{y_{c,T}}{2}, p_{c,A} \right) f_B \left(X_c - \frac{y_{c,T}}{2}, p_{c,B} \right) \\ &\quad \times \exp [i(\mathbf{k}'_{c,A} - \mathbf{k}_{c,A}) \cdot \mathbf{b}_c] \\ &\quad \times \sum_{s_A, s_B, s_1, s_2} 2s_2 \mathbf{n}_c \mathcal{M} (\{s_A, k_{c,A}; s_B, k_{c,B}\} \rightarrow \{s_1, p_{c,1}; s_2, p_{c,2}\}) \\ &\quad \times \mathcal{M}^* (\{s_A, k'_{c,A}; s_B, k'_{c,B}\} \rightarrow \{s_1, p_{c,1}; s_2, p_{c,2}\}), \end{aligned} \quad (69)$$

where $\mathbf{P}_{AB \rightarrow 12}$ denotes the polarization vector of particle 2; ϕ_A and ϕ_B are the wave packets for A and B , respectively; $\mathbf{n}_c = \hat{\mathbf{b}}_c \times \hat{\mathbf{p}}_{c,A}$ is the direction of the reaction plane in the center-of-mass frame, with $\hat{\mathbf{b}}_c$ being the unit impact parameter vector; f_A and f_B are the distributions at the coordinates $X_c + y_{c,T}/2$ and $X_c - y_{c,T}/2$, respectively; and \mathcal{M} denotes the amplitude of the 2-to-2 scattering with all the spins and momenta specified. All the momenta are defined in the center-of-mass frame and indicated by the index c . For more details on (69), see Ref. [171]. The wave packets ensure that the colliding particles have a non-vanishing initial angular momentum; the matrix elements encode the collision probability, and the spin projection and Lorentz transformation provide a consistent treatment of particle scattering in the thermal bath frame. One can apply (69) to the quark–gluon system. Then the quark polarization rate per unit volume with all the 2-to-2 parton scatterings in a locally thermalized QGP in momentum is

$$\begin{aligned} \frac{d^4 \mathbf{P}_q(X)}{dX^4} &= \frac{\pi}{(2\pi)^4} \frac{\partial(\beta u_\rho)}{\partial X^\nu} \sum_{A,B,1} \int \frac{d^3 p_A}{(2\pi)^3 2E_A} \frac{d^3 p_B}{(2\pi)^3 2E_B} \\ &\quad \times |v_{c,A} - v_{c,B}| [\Lambda^{-1}]_j^\nu \mathbf{e}_{c,i} \epsilon_{ikh} \hat{\mathbf{p}}_{c,A}^h \\ &\quad \times f_A(X, p_A) f_B(X, p_B) (p_A^\rho - p_B^\rho) \Theta_{jk}(\mathbf{p}_{c,A}) \\ &\equiv \frac{\partial(\beta u_\rho)}{\partial X^\nu} \mathbf{W}^{\rho\nu}, \end{aligned} \quad (70)$$

which is proportional to the thermal vorticity. Here the tensor $\mathbf{W}^{\rho\nu}$ contains 64 components, each of which involves a 16-dimensional integration. The numerical calculation of $\mathbf{W}^{\rho\nu}$ is challenging owing to the very large number of scattering amplitudes and high-dimensional collision integrals. To tackle this problem, a new Monte-Carlo integration algorithm, ZMCintegral, which can handle 16-dimensional integration, has been developed for use on multiple GPUs [172, 173]. The most recent application of this algorithm is the solution of the Boltzmann equations of a partonic system [174]. The numerical result shows that $\mathbf{W}^{\rho\nu}$ has an antisymmetric form:

$$\mathbf{W}^{\rho\nu} = \begin{pmatrix} 0 & 0 & 0 & 0 \\ 0 & 0 & W \mathbf{e}_z & -W \mathbf{e}_y \\ 0 & -W \mathbf{e}_z & 0 & W \mathbf{e}_x \\ 0 & W \mathbf{e}_y & -W \mathbf{e}_x & 0 \end{pmatrix}, \quad (71)$$

where W is approximately constant. Note that W depends on the cutoff of the impact parameter, as shown in Fig. 8. Finally, the polarization rate per unit volume for one quark flavor can be expressed compactly:

$$\frac{d^4 \mathbf{P}_q(X)}{dX^4} = 2W \nabla_X \times \left(\frac{\mathbf{u}}{T} \right). \quad (72)$$

This is a good example of how spin–vorticity coupling emerges naturally from particle scattering.

Note that the result of Ref. [171] or Eq. (70) does not include the back reaction to contain the growing polarization with increasing vorticity in the absence of a cutoff. A systematic derivation of the spin polarization from the vorticity through non-local collisions with back reactions has been performed [175] by expanding the collision terms in the Planck constant for massive fermions [121].

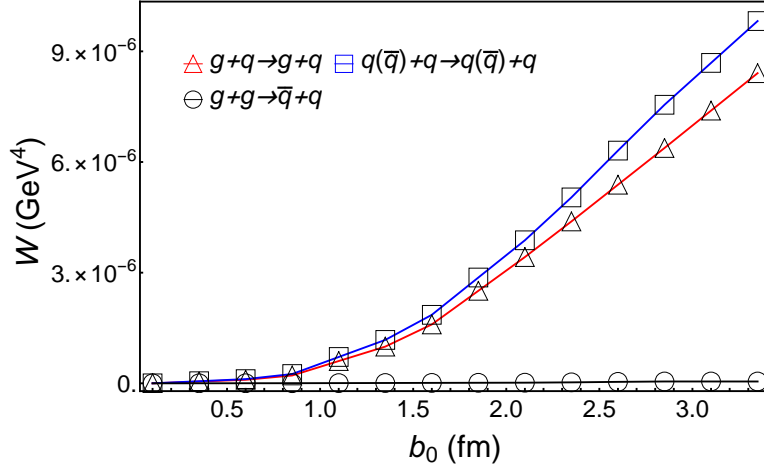
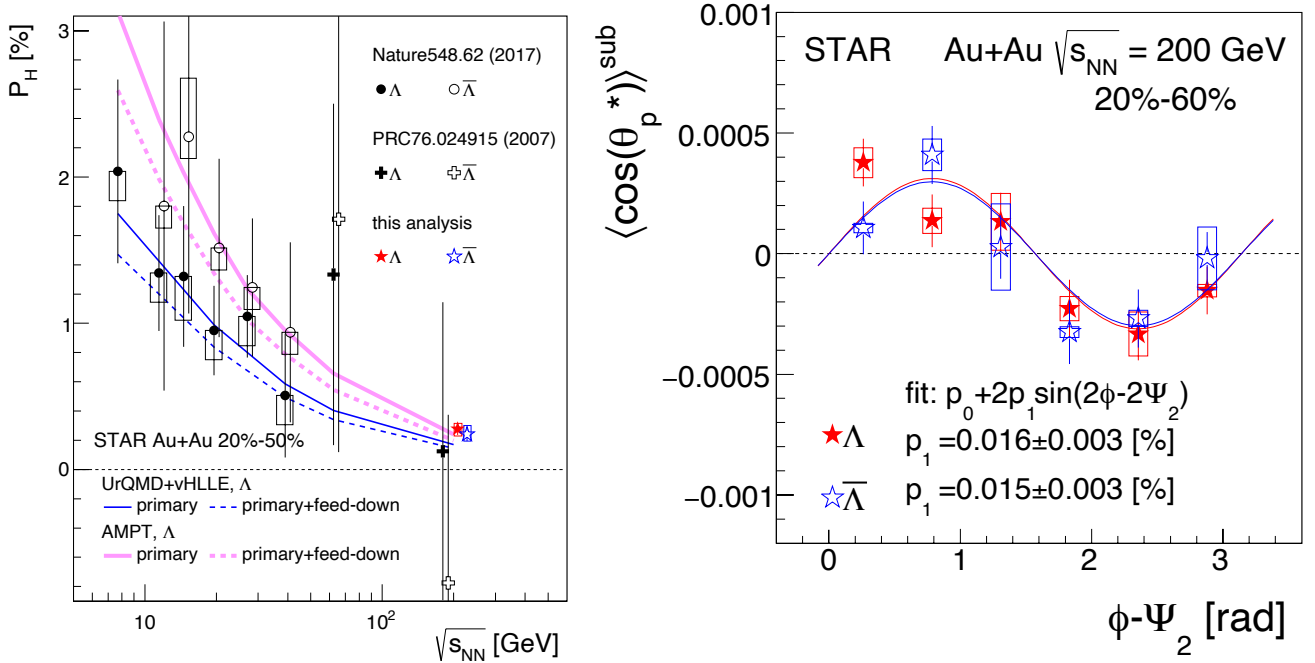
B. Experimental results

The global polarization of Λ hyperons can be measured through their weak decays. The angular distribution of the daughter baryons is [5, 111]

$$\frac{dN}{d \cos \theta^*} = \frac{1}{2} (1 + \alpha_H P_H \cos \theta^*), \quad (73)$$

where α_H is the decay constant of the hyperon, P_H is the polarization of the hyperon (a fraction), and θ^* is the angle between the momentum of the daughter baryon and the polarization direction in the hyperon rest frame. The experimental results for the global polarization of Λ and $\bar{\Lambda}$ hyperons measured by the STAR Collaboration [5, 111] are shown in the left panel of Fig. 9. $P_H(\Lambda)$ and $P_H(\bar{\Lambda})$ decrease with the collision energy. From the data, the fluid vorticity can be estimated as $\omega \simeq k_B T (P_\Lambda + P_{\bar{\Lambda}}) / \hbar$ [176]. It also appears that $P_H(\bar{\Lambda}) \gtrsim P_H(\Lambda)$, although the difference is not significant; this result may suggest a possible contribution from the magnetic field or other effects [177, 178]. The data can be described by various phenomenological models using (44) [105, 142, 143, 179–181].

The right panel of Fig. 9 shows the recent STAR Collaboration measurement [21] of the longitudinal polarization as a function of the azimuthal angle ϕ relative to the second-order event plane Ψ_2 . The longitudinal spin polarization data show

Fig. 8. Numerical results for W as a function of b_0 , the cutoff for $|\mathbf{b}_c|$.Fig. 9. Global polarization of Λ and $\bar{\Lambda}$ (left panel) [5, 111] and local polarization as a function of azimuthal angle ϕ relative to the second-order event plane Ψ_2 (right panel) [21] measured by STAR.

positive $\sin(2\phi - 2\Psi_2)$ behavior, whereas the theoretical results of the relativistic hydrodynamics model [182] and transport models [143, 180, 183] show the opposite sign along the beam line direction. A simulation using CKT [110] and the results obtained using a simple phenomenological model [184] give the correct sign as the data. The azimuthal angle dependence of the spin polarization in the direction of the global OAM has been measured by the STAR Collaboration. Some phenomenological models do not well describe the STAR data for the azimuthal angle dependence of the global polarization.

The sign problem of the local polarization requires further investigations. It may indicate a need for new frameworks to describe the spin dynamics, such as the quantum spin kinetic theory for massive particles (see Sec. III) or the spin hydrodynamics (see Sec. IV A).

One possible effect is that of feed-down decays. The hyperons measured in experiments may be produced by decays of heavier resonance particles. However, the authors of Refs. [185, 186] concluded that feed-down effects decreased by approximately 10% for the Λ primordial spin polarization; thus, they do not solve the spin sign problem.

In addition, the sign problem of the local polarization may also indicate that the assumption of global or local equilibrium of the spin may not be justified, and thus the thermal vorticity may not be the correct quantity for the spin chemical potential.

Wu *et al.* [148, 149] tested four different types of vorticity: the kinematic vorticity, relativistic extension of the non-relativistic vorticity, temperature vorticity, and thermal vorticity. They calculated the local polarization of hyperons corresponding to each type of vorticity. By using the $(3 + 1)$ -dimensional hydrodynamic model with the AMPT initial conditions encoding the global OAM, they found a few remarkable differences between the results for different vorticities. First, although all four types of vorticity give the correct sign and magnitude of the polarization along the global OAM direction, only the temperature vorticity agrees with the STAR preliminary result in showing a decreasing trend of the azimuthal angle dependence. Second, only the temperature vorticity can simultaneously provide the correct sign and magnitude of the longitudinal polarization. This result suggests the possibility of spin–temperature vorticity coupling, analogous to magnetic moment–magnetic field coupling. It is also possible that the agreement may be a coincidental result of the main assumption that the spin vector depends on the temperature vorticity in the same way as it does on the thermal vorticity. Further investigation is needed to clarify why the results for the temperature vorticity are the most satisfactory.

The vector meson spin alignment is another recent research topic. The spin alignment of a vector meson is described by the 3×3 Hermitian spin-density matrix [187, 188]. The 00-component of the spin-density matrix enters the angular distribution of its decay daughter as

$$\frac{dN}{d \cos \theta^*} \propto [(1 - \rho_{00}) + (3\rho_{00} - 1) \cos^2 \theta^*], \quad (74)$$

where θ^* is the angle between the decay daughter and the spin quantization direction in the vector meson's rest frame. Thus, the ρ_{00} value of the vector meson can be measured using the angular distribution of its decay daughter. The vector meson (K^{*0} and ϕ) spin alignments have been measured by the ALICE Collaboration [189]. The ρ_{00} value is consistent with $1/3$ for both K^{*0} and ϕ mesons in p+p collisions. In Pb+Pb collisions, the ρ_{00} value of K^{*0} is approximately $1/3$ at high p_T and less than $1/3$ at low p_T .

Theoretical calculations using the statistical-hydro model [176] and quark coalescence model [190] give

$$\rho_{00}^\phi \approx \frac{1}{3} - \frac{4}{9} P_\Lambda P_{\bar{\Lambda}} \lesssim \frac{1}{3}. \quad (75)$$

Using the STAR data, $P_\Lambda \approx (1.08 \pm 0.15 \pm 0.11)\%$ and $P_{\bar{\Lambda}} \approx (1.38 \pm 0.30 \pm 0.13)\%$ [5, 111], one can estimate $(4/9)P_\Lambda P_{\bar{\Lambda}} \approx 6.6 \times 10^{-5}$, which may suggest that ρ_{00}^ϕ cannot be significantly larger than $1/3$ and thus contradict the STAR preliminary data for ρ_{00}^ϕ .

To solve this puzzle, it is proposed that a strangeness current can exist in heavy-ion collisions and give rise to a non-vanishing mean ϕ field [191]. Like the magnetic field, the magnetic part of the ϕ field can also polarize s and \bar{s} through their magnetic moments; this polarization contributes to the polarization of Λ and $\bar{\Lambda}$, whereas the contribution from the electric part of the ϕ field is absent and therefore is not constrained by the polarization of Λ and $\bar{\Lambda}$. However, the electric part of the ϕ field contributes significantly to ρ_{00}^ϕ , which is positive definite [191]:

$$\rho_{00}^\phi \approx \frac{1}{3} + \frac{g_\phi^2}{27m_s^4 T_{\text{eff}}^2} \langle \mathbf{p}^2 \rangle_\phi \langle E_{\phi,z}^2 + E_{\phi,x}^2 \rangle, \quad (76)$$

where \mathbf{E}_ϕ is the electric part of the ϕ field, m_s is the strange quark mass, $\langle \mathbf{p}^2 \rangle_\phi$ is the mean value of \mathbf{p}^2 for s or \bar{s} in the ϕ meson wave function, g_ϕ is the coupling constant of the s quark to the ϕ meson in the quark–meson model, and T_{eff} is the average temperature of the fireball. The contribution originates from the spin–orbit coupling term that polarizes s and \bar{s} . Thus, one can see that ρ_{00} for the ϕ meson is a good tool for analyzing the ϕ mean field even if it may strongly fluctuate in space-time [191]. The theoretical prediction of ρ_{00}^ϕ as a function of the collision energy is shown in Fig. 10.

However, this theory does not work for another vector meson, K^{*0} , for several reasons. First, because of the unequal masses of \bar{s} and d , one cannot derive the same formula as that for ϕ mesons, in which the contributions from the vorticity and those from the electric and magnetic fields are decoupled. Second, the interaction of K^{*0} with the surrounding matter is much stronger than that of the ϕ meson. The above points are supported by preliminary data from ALICE [189].

V. SUMMARY

We gave a brief overview of recent theoretical developments and experimental results on the effects of chirality and vorticity on heavy-ion collisions. We focus on works reported at the Quark Matter conference of 2019.

We discussed the time evolution of magnetic fields in various models of the QGP, for example, the Lienard–Wiechert potential and MHD models. Macroscopic models such as the second-order dissipative MHD and AVFD models are applied in phenomenological studies.

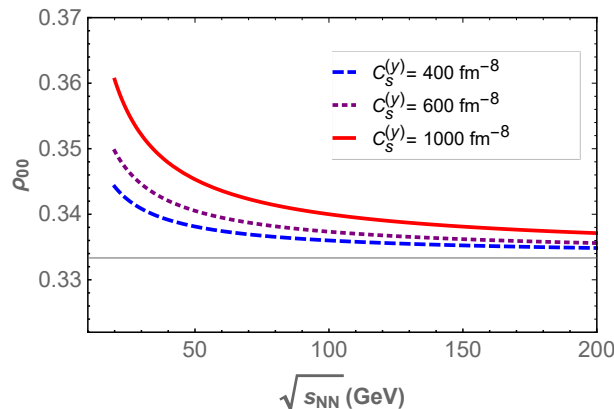


Fig. 10. Theoretical prediction of ρ_{00}^{ϕ} in heavy-ion collisions as a function of collision energy. The thin horizontal solid line shows the no-alignment value, $\rho_{00} = 1/3$. Three values of $C_s^{(y)}$ are chosen [191].

It is still experimentally challenging to obtain a clear CME signal against the dominant backgrounds. The non-flow correlations for the CMW give rise to additional backgrounds in the slope of $\Delta v_2(A_{ch})$. More detailed studies of the CME and CMW are needed.

The kinetic theory of massive fermions has been developed for the covariant and equal-time Wigner functions and the Schwinger–Keldysh formalism. The collision terms have been studied at the leading and next-to-leading order in an expansion of the Planck constant.

The decomposition of the total angular momentum into the OAM and spin has been debated for quite a long time. Another important issue that remains to be resolved is the relationship between the theoretical spin and the results of experimental measurements.

For the global polarization of Λ and $\bar{\Lambda}$ hyperons, various phenomenological models give consistent descriptions of the experimental data. For the local polarization, the nature of the spin sign problem is still unclear. It has been proposed that a significant positive deviation of $1/3$ for ρ_{00}^{ϕ} may indicate the existence of a mean ϕ field.

ACKNOWLEDGMENTS

J.-H.G. is supported in part by the National Natural Science Foundation of China under Grant No. 11890713. G.-L.M. is supported by the National Natural Science Foundation of China under Grant Nos. 11890714, 11835002, 11961131011, and 11421505, and the Strategic Priority Research Program of the Chinese Academy of Sciences under Grant No. XDB34030202. Q.-W. is supported in part by the National Natural Science Foundation of China under Grant Nos. 11535012 and 11890713, and the Strategic Priority Research Program of the Chinese Academy of Sciences under Grant No. XDB34030102.

-
- [1] J. Błoczynski, X.-G. Huang, X. Zhang, and J. Liao, Azimuthally fluctuating magnetic field and its impacts on observables in heavy-ion collisions, *Phys. Lett.* **B718**, 1529 (2013), doi: [10.1016/j.physletb.2012.12.030](https://doi.org/10.1016/j.physletb.2012.12.030).
 - [2] W.-T. Deng and X.-G. Huang, Event-by-event generation of electromagnetic fields in heavy-ion collisions, *Phys. Rev.* **C85**, 044907 (2012), doi: [10.1103/PhysRevC.85.044907](https://doi.org/10.1103/PhysRevC.85.044907).
 - [3] V. Roy and S. Pu, Event-by-event distribution of magnetic field energy over initial fluid energy density in $\sqrt{s_{NN}} = 200$ GeV Au-Au collisions, *Phys. Rev.* **C92**, 064902 (2015), doi: [10.1103/PhysRevC.92.064902](https://doi.org/10.1103/PhysRevC.92.064902).
 - [4] H. Li, X.-l. Sheng, and Q. Wang, Electromagnetic fields with electric and chiral magnetic conductivities in heavy ion collisions, *Phys. Rev.* **C94**, 044903 (2016), doi: [10.1103/PhysRevC.94.044903](https://doi.org/10.1103/PhysRevC.94.044903).
 - [5] STAR, L. Adamczyk *et al.*, Global Λ hyperon polarization in nuclear collisions: evidence for the most vortical fluid, *Nature* **548**, 62 (2017), doi: [10.1038/nature23004](https://doi.org/10.1038/nature23004).
 - [6] D. Kharzeev, Parity violation in hot QCD: Why it can happen, and how to look for it, *Phys. Lett.* **B633**, 260 (2006), doi: [10.1016/j.physletb.2005.11.075](https://doi.org/10.1016/j.physletb.2005.11.075).
 - [7] D. E. Kharzeev, L. D. McLerran, and H. J. Warringa, The Effects of topological charge change in heavy ion collisions: 'Event by event P and CP violation', *Nucl. Phys.* **A803**, 227 (2008), doi: [10.1016/j.nuclphysa.2008.02.298](https://doi.org/10.1016/j.nuclphysa.2008.02.298).
 - [8] K. Fukushima, D. E. Kharzeev, and H. J. Warringa, The Chiral Magnetic Effect, *Phys. Rev.* **D78**, 074033 (2008), doi: [10.1103/PhysRevD.78.074033](https://doi.org/10.1103/PhysRevD.78.074033).

- [9] Q. Li *et al.*, Observation of the chiral magnetic effect in ZrTe₅, *Nature Phys.* **12**, 550 (2016), doi:10.1038/nphys3648 .
- [10] D. E. Kharzeev and Q. Li, The Chiral Qubit: quantum computing with chiral anomaly, (2019), in preparation, arXiv: 1903.07133.
- [11] D. E. Kharzeev, J. Liao, S. A. Voloshin, and G. Wang, Chiral magnetic and vortical effects in high energy nuclear collisions: A status report, *Prog. Part. Nucl. Phys.* **88**, 1 (2016), doi: 10.1016/j.pnpnp.2016.01.001.
- [12] J. Liao, Anomalous transport effects and possible environmental symmetry ‘violation’ in heavy-ion collisions, *Pramana* **84**, 901 (2015), doi:10.1007/s12043-015-0984-x.
- [13] V. A. Miransky and I. A. Shovkovy, Quantum field theory in a magnetic field: From quantum chromodynamics to graphene and Dirac semimetals, *Phys. Rept.* **576**, 1 (2015), doi:10.1016/j.physrep.2015.02.003.
- [14] X.-G. Huang, Electromagnetic fields and anomalous transports in heavy-ion collisions — A pedagogical review, *Rept. Prog. Phys.* **79**, 076302 (2016), doi:10.1088/0034-4885/79/7/076302.
- [15] V. Koch, S. Schlichting, V. Skokov, P. Sorensen, J. Thomas, S. Voloshin, G. Wang and H. U. Yee, Status of the chiral magnetic effect and collisions of isobars, *Chin. Phys. C* **41**,072001 (2017) doi:10.1088/1674-1137/41/7/072001.
- [16] K. Fukushima, Extreme matter in electromagnetic fields and rotation, *Prog. Part. Nucl. Phys.* **107**, 167 (2019), doi:10.1016/j.pnpnp.2019.04.001.
- [17] A. Bzdak *et al.*, Mapping the Phases of Quantum Chromodynamics with Beam Energy Scan, in preparation, arXiv:1906.00936.
- [18] J. Zhao and F. Wang, Experimental searches for the chiral magnetic effect in heavy-ion collisions, *Prog. Part. Nucl. Phys.* **107**, 200 (2019), doi:10.1016/j.pnpnp.2019.05.001.
- [19] F. Q. Wang and J. Zhao, Search for the chiral magnetic effect in heavy ion collisions, *Nucl. Sci. Tech.* **29**, 179 (2018) doi:10.1007/s41365-018-0520-z.
- [20] Y. C. Liu and X. G. Huang, Anomalous chiral transports and spin polarization in heavy-ion collisions,” *Nucl. Sci. Tech.* **31**,56 (2020) doi:10.1007/s41365-020-00764-z.
- [21] STAR, J. Adam *et al.*, Polarization of Λ ($\bar{\Lambda}$) hyperons along the beam direction in Au+Au collisions at $\sqrt{s_{NN}} = 200$ GeV, *Phys. Rev. Lett.* **123**, 132301 (2019), doi:10.1103/PhysRevLett.123.132301.
- [22] L. McLerran and V. Skokov, Comments About the Electromagnetic Field in Heavy-Ion Collisions, *Nucl. Phys.* **A929**, 184 (2014), doi:10.1016/j.nuclphysa.2014.05.008.
- [23] U. Gürsoy, D. Kharzeev, and K. Rajagopal, Magnetohydrodynamics, charged currents and directed flow in heavy ion collisions, *Phys. Rev. C* **89**, 054905 (2014), doi:10.1103/PhysRevC.89.054905.
- [24] U. Gürsoy, D. Kharzeev, E. Marcus, K. Rajagopal, and C. Shen, Charge-dependent Flow Induced by Magnetic and Electric Fields in Heavy Ion Collisions, *Phys. Rev.* **C98**, 055201 (2018), doi:10.1103/PhysRevC.98.055201.
- [25] S. Pu, V. Roy, L. Rezzolla, and D. H. Rischke, Bjorken flow in one-dimensional relativistic magnetohydrodynamics with magnetization, *Phys. Rev.* **D93**, 074022 (2016), doi:10.1103/PhysRevD.93.074022.
- [26] V. Roy, S. Pu, L. Rezzolla, and D. Rischke, Analytic Bjorken flow in one-dimensional relativistic magnetohydrodynamics, *Phys. Lett.* **B750**, 45 (2015), doi:10.1016/j.physletb.2015.08.046.
- [27] S. Pu and D.-L. Yang, Transverse flow induced by inhomogeneous magnetic fields in the Bjorken expansion, *Phys. Rev.* **D93**, 054042 (2016), doi:10.1103/PhysRevD.93.054042.
- [28] S. Pu and D.-L. Yang, Analytic Solutions of Transverse Magneto-hydrodynamics under Bjorken Expansion, *EPJ Web Conf.* **137**, 13021 (2017), doi:10.1051/epjconf/201713713021.
- [29] V. Roy, S. Pu, L. Rezzolla, and D. H. Rischke, Effect of intense magnetic fields on reduced-MHD evolution in $\sqrt{s_{NN}} = 200$ GeV Au+Au collisions, *DAE Symp. Nucl. Phys.* **62**, 926 (2017).
- [30] I. Siddique, R.-j. Wang, S. Pu, and Q. Wang, Anomalous magnetohydrodynamics with longitudinal boost invariance and chiral magnetic effect, *Phys. Rev.* **D99**, 114029 (2019), doi:10.1103/PhysRevD.99.114029.
- [31] R.-j. Wang, P. Copinger, and S. Pu, Anomalous magnetohydrodynamics with constant anisotropic electric conductivities, in *28th International Conference on Ultrarelativistic Nucleus-Nucleus Collisions*, in preparation, arXiv:2004.06408.
- [32] G. Inghirami *et al.*, Numerical magneto-hydrodynamics for relativistic nuclear collisions, *Eur. Phys. J.* **C76**, 659 (2016), doi:10.1140/epjc/s10052-016-4516-8.
- [33] G. Inghirami *et al.*, Magnetic fields in heavy ion collisions: flow and charge transport, in preparation, arXiv:1908.07605.
- [34] L.-G. Pang, G. Endr^oodi, and H. Petersen, Magnetic-field-induced squeezing effect at energies available at the BNL Relativistic Heavy Ion Collider and at the CERN Large Hadron Collider, *Phys. Rev. C* **93**, 044919 (2016), doi:10.1103/PhysRevC.93.044919.
- [35] G. S. Denicol *et al.*, Nonresistive dissipative magnetohydrodynamics from the Boltzmann equation in the 14-moment approximation, *Phys. Rev.* **D98**, 076009 (2018), doi:10.1103/PhysRevD.98.076009.
- [36] G. S. Denicol, E. Molnár, H. Niemi, and D. H. Rischke, Resistive dissipative magnetohydrodynamics from the Boltzmann-Vlasov equation, *Phys. Rev.* **D99**, 056017 (2019), doi:10.1103/PhysRevD.99.056017.
- [37] S. Shi, C. Gale, and S. Jeon, From Chiral Kinetic Theory To Spin Hydrodynamics, in *28th International Conference on Ultrarelativistic Nucleus-Nucleus Collisions (Quark Matter 2019) Wuhan, China, November 4-9, 2019*, in preparation, arXiv:2002.01911.
- [38] B. Müller and A. Schäfer, Chiral magnetic effect and an experimental bound on the late time magnetic field strength, *Phys. Rev.* **D98**, 071902 (2018), doi:10.1103/PhysRevD.98.071902.
- [39] Y. Guo, S. Shi, S. Feng, and J. Liao, Magnetic Field Induced Polarization Difference between Hyperons and Anti-hyperons, *Phys. Lett.* **B798**, 134929 (2019), doi:10.1016/j.physletb.2019.134929.
- [40] L. Huang, C.-W. Ma, and G.-L. Ma, Investigating the quark flavor dependence of the chiral magnetic effect with a multiphase transport model, *Phys. Rev. C* **97**, 034909 (2018), doi:10.1103/PhysRevC.97.034909.
- [41] W.-T. Deng, X.-G. Huang, G.-L. Ma, and G. Wang, Predictions for isobaric collisions at $\sqrt{s_{NN}} = 200$ GeV from a multiphase transport model, *Phys. Rev. C* **97**, 044901 (2018), doi:10.1103/PhysRevC.97.044901.

- [42] X.-L. Zhao, G.-L. Ma, and Y.-G. Ma, Impact of magnetic-field fluctuations on measurements of the chiral magnetic effect in collisions of isobaric nuclei, *Phys. Rev. C* **99**, 034903 (2019), doi:10.1103/PhysRevC.99.034903.
- [43] L. Huang, M.-W. Nie, and G.-L. Ma, Sensitivity analysis of the chiral magnetic effect observables using a multiphase transport model, *Phys. Rev. C* **101**, 024916 (2020), doi:10.1103/PhysRevC.101.024916.
- [44] N. Magdy, M.-W. Nie, G.-L. Ma, and R. A. Lacey, A sensitivity study of the primary correlators used to characterize chiral-magnetically-driven charge separation, (2020), in preparation, arXiv:2002.07934.
- [45] Y. Jiang, S. Shi, Y. Yin, and J. Liao, Quantifying the chiral magnetic effect from anomalous-viscous fluid dynamics, *Chin. Phys.* **C42**, 011001 (2018), doi:10.1088/1674-1137/42/1/011001.
- [46] S. Shi, Y. Jiang, E. Lilleskov, and J. Liao, Anomalous Chiral Transport in Heavy Ion Collisions from Anomalous-Viscous Fluid Dynamics, *Annals Phys.* **394**, 50 (2018), doi:10.1016/j.aop.2018.04.026.
- [47] S. Shi, Y. Jiang, E. Lilleskov, and J. Liao, Quantification of Chiral Magnetic Effect from Event-by-Event Anomalous-Viscous Fluid Mechanics, *PoS CPOD2017*, 021 (2018), doi:10.22323/1.311.0021.
- [48] B. Schenke, C. Shen, and P. Tribedy, Multi-particle and charge-dependent azimuthal correlations in heavy-ion collisions at the Relativistic Heavy-Ion Collider, *Phys. Rev.* **C99**, 044908 (2019), doi:10.1103/PhysRevC.99.044908.
- [49] D. Oliinychenko and V. Koch, Microcanonical Particlization with Local Conservation Laws, *Phys. Rev. Lett.* **123**, 182302 (2019), doi:10.1103/PhysRevLett.123.182302.
- [50] S. Shi, H. Zhang, D. Hou, and J. Liao, Signatures of Chiral Magnetic Effect in the Collisions of Isobars, (2019), in preparation, arXiv:1910.14010.
- [51] K. Fukushima, D. E. Kharzeev, and H. J. Warringa, Real-time dynamics of the Chiral Magnetic Effect, *Phys. Rev. Lett.* **104**, 212001 (2010), doi:10.1103/PhysRevLett.104.212001.
- [52] J. S. Schwinger, On gauge invariance and vacuum polarization, *Phys. Rev.* **82**, 664 (1951), doi:10.1103/PhysRev.82.664.
- [53] P. Copinger, K. Fukushima, and S. Pu, Axial Ward identity and the Schwinger mechanism – Applications to the real-time chiral magnetic effect and condensates, *Phys. Rev. Lett.* **121**, 261602 (2018), doi:10.1103/PhysRevLett.121.261602.
- [54] B. Feng *et al.*, Chiral Magnetic Effect in a Lattice Model, *Phys. Rev. D* **95**, 114023 (2017), doi:10.1103/PhysRevD.95.114023.
- [55] Y. Wu, D. Hou, and H.-c. Ren, Field theoretic perspectives of the Wigner function formulation of the chiral magnetic effect, *Phys. Rev. D* **96**, 096015 (2017), doi:10.1103/PhysRevD.96.096015.
- [56] S. Lin and L. Yang, Mass correction to chiral vortical effect and chiral separation effect, *Phys. Rev. D* **98**, 114022 (2018), doi:10.1103/PhysRevD.98.114022.
- [57] M. Horvath, D. Hou, J. Liao, and H.-c. Ren, Chiral magnetic response to arbitrary axial imbalance, *Phys. Rev. D* **101**, 076026 (2020), doi:10.1103/PhysRevD.101.076026.
- [58] B. Feng, D.-F. Hou, and H.-C. Ren, QED radiative corrections to chiral magnetic effect, *Phys. Rev. D* **99**, 036010 (2019), doi:10.1103/PhysRevD.99.036010.
- [59] D.-f. Hou and S. Lin, Fluctuation and Dissipation of Axial Charge from Massive Quarks, *Phys. Rev. D* **98**, 054014 (2018), doi:10.1103/PhysRevD.98.054014.
- [60] S. Lin, L. Yan, and G.-R. Liang, Axial Charge Fluctuation and Chiral Magnetic Effect from Stochastic Hydrodynamics, *Phys. Rev. C* **98**, 014903 (2018), doi:10.1103/PhysRevC.98.014903.
- [61] S. A. Voloshin, Parity violation in hot QCD: How to detect it, *Phys. Rev.* **C70**, 057901 (2004), doi:10.1103/PhysRevC.70.057901.
- [62] ALICE, B. Abelev *et al.*, Charge separation relative to the reaction plane in Pb-Pb collisions at $\sqrt{s_{NN}} = 2.76$ TeV, *Phys. Rev. Lett.* **110**, 012301 (2013), doi:10.1103/PhysRevLett.110.012301.
- [63] ALICE, S. Aziz, Search for the Chiral Magnetic Effect with the ALICE detector, in *28th International Conference on Ultrarelativistic Nucleus-Nucleus Collisions (Quark Matter 2019) Wuhan, China, November 4-9, 2019*, in preparation, arXiv:2005.06177.
- [64] W.-T. Deng, X.-G. Huang, G.-L. Ma, and G. Wang, Test the chiral magnetic effect with isobaric collisions, *Phys. Rev.* **C94**, 041901 (2016), doi:10.1103/PhysRevC.94.041901.
- [65] A. Bzdak and V. Skokov, Event-by-event fluctuations of magnetic and electric fields in heavy ion collisions, *Phys. Lett.* **B710**, 171 (2012), doi:10.1016/j.physletb.2012.02.065.
- [66] STAR, J. Zhao, Search for CME in U+U and Au+Au collisions in STAR with different approaches of handling backgrounds, in preparation, arXiv:2002.09410.
- [67] H.-j. Xu *et al.*, Varying the chiral magnetic effect relative to flow in a single nucleus-nucleus collision, *Chin. Phys.* **C42**, 084103 (2018), doi:10.1088/1674-1137/42/8/084103.
- [68] CMS, V. Khachatryan *et al.*, Observation of charge-dependent azimuthal correlations in p -Pb collisions and its implication for the search for the chiral magnetic effect, *Phys. Rev. Lett.* **118**, 122301 (2017), doi:10.1103/PhysRevLett.118.122301.
- [69] CMS, A. M. Sirunyan *et al.*, Constraints on the chiral magnetic effect using charge-dependent azimuthal correlations in p Pb and PbPb collisions at the CERN Large Hadron Collider, *Phys. Rev.* **C97**, 044912 (2018), doi:10.1103/PhysRevC.97.044912.
- [70] STAR, Y. Lin, Measurement of the charge separation along the magnetic field with Signed Balance Function in 200 GeV Au + Au collisions at STAR, in *28th International Conference on Ultrarelativistic Nucleus-Nucleus Collisions (Quark Matter 2019) Wuhan, China, November 4-9, 2019*, in preparation, arXiv: 2002.11446.
- [71] A. Bzdak, V. Koch, and J. Liao, Charge-Dependent Correlations in Relativistic Heavy Ion Collisions and the Chiral Magnetic Effect, *Lect. Notes Phys.* **871**, 503 (2013), doi:10.1007/978-3-642-37305-3-19.
- [72] STAR, J. Adam *et al.*, Pair invariant mass to isolate background in the search for the chiral magnetic effect in Au+Au collisions at $\sqrt{s_{NN}} = 200$ GeV, in preparation, arXiv:2006.05035.
- [73] W. Li and G. Wang, Chiral Magnetic Effects in Nuclear Collisions, in preparation, arXiv:2002.10397.
- [74] A. H. Tang, Probe Chiral Magnetic Effect with Signed Balance Function, in preparation, arXiv:1903.04622.

- [75] J. Adam *et al.* [STAR], Charge separation measurements in $p(d)+\text{Au}$ and $\text{Au}+\text{Au}$ collisions; implications for the chiral magnetic effect, in preparation, [arXiv:2006.04251](https://arxiv.org/abs/2006.04251).
- [76] N. Magdy, S. Shi, J. Liao, N. Ajitanand, and R. A. Lacey, New correlator to detect and characterize the chiral magnetic effect, *Phys. Rev.* **C97**, 061901 (2018), [doi:10.1103/PhysRevC.97.061901](https://doi.org/10.1103/PhysRevC.97.061901).
- [77] N. Magdy, S. Shi, J. Liao, P. Liu, and R. A. Lacey, Examination of the observability of a chiral magnetically driven charge-separation difference in collisions of the $^{96}_{44}\text{Ru} + ^{96}_{44}\text{Ru}$ and $^{96}_{40}\text{Zr} + ^{96}_{40}\text{Zr}$ isobars at energies available at the BNL Relativistic Heavy Ion Collider, *Phys. Rev.* **C98**, 061902 (2018), [doi:10.1103/PhysRevC.98.061902](https://doi.org/10.1103/PhysRevC.98.061902).
- [78] X.-L. Zhao, Y.-G. Ma, and G.-L. Ma, Electromagnetic fields in small systems from a multiphase transport model, *Phys. Rev.* **C97**, 024910 (2018), [doi:10.1103/PhysRevC.97.024910](https://doi.org/10.1103/PhysRevC.97.024910).
- [79] STAR, L. Adamczyk *et al.*, Observation of charge asymmetry dependence of pion elliptic flow and the possible chiral magnetic wave in heavy-ion collisions, *Phys. Rev. Lett.* **114**, 252302 (2015), [doi:10.1103/PhysRevLett.114.252302](https://doi.org/10.1103/PhysRevLett.114.252302).
- [80] H.-J. Xu *et al.*, Importance of isobar density distributions on the chiral magnetic effect search, *Phys. Rev. Lett.* **121**, 022301 (2018), [doi:10.1103/PhysRevLett.121.022301](https://doi.org/10.1103/PhysRevLett.121.022301).
- [81] H.-j. Xu, J. Zhao, Y. Feng, and F. Wang, Importance of non-flow background on the chiral magnetic wave search, in *28th International Conference on Ultrarelativistic Nucleus-Nucleus Collisions (Quark Matter 2019) Wuhan, China, November 4-9, 2019*, in preparation, [arXiv:2002.05220](https://arxiv.org/abs/2002.05220).
- [82] D. E. Kharzeev and H.-U. Yee, Chiral Magnetic Wave, *Phys. Rev.* **D83**, 085007 (2011), [doi:10.1103/PhysRevD.83.085007](https://doi.org/10.1103/PhysRevD.83.085007).
- [83] Y. Burnier, D. E. Kharzeev, J. Liao, and H.-U. Yee, Chiral magnetic wave at finite baryon density and the electric quadrupole moment of quark-gluon plasma in heavy ion collisions, *Phys. Rev. Lett.* **107**, 052303 (2011), [doi:10.1103/PhysRevLett.107.052303](https://doi.org/10.1103/PhysRevLett.107.052303).
- [84] G.-L. Ma, Final state effects on charge asymmetry of pion elliptic flow in high-energy heavy-ion collisions, *Phys. Lett.* **B735**, 383 (2014), [doi:10.1016/j.physletb.2014.06.074](https://doi.org/10.1016/j.physletb.2014.06.074).
- [85] H.-j. Xu, J. Zhao, Y. Feng, and F. Wang, Complications in the interpretation of the charge asymmetry dependent π flow for the chiral magnetic wave, *Phys. Rev.* **C101**, 014913 (2020), [doi:10.1103/PhysRevC.101.014913](https://doi.org/10.1103/PhysRevC.101.014913).
- [86] STAR, Q.-Y. Shou, Search for the Chiral Magnetic Wave with Anisotropic Flow of Identified Particles at RHIC-STAR, *Nucl. Phys.* **A982**, 555 (2019), [doi:10.1016/j.nuclphysa.2018.09.016](https://doi.org/10.1016/j.nuclphysa.2018.09.016).
- [87] M. A. Stephanov and Y. Yin, Chiral Kinetic Theory, *Phys. Rev. Lett.* **109**, 162001 (2012), [doi:10.1103/PhysRevLett.109.162001](https://doi.org/10.1103/PhysRevLett.109.162001).
- [88] D. T. Son and N. Yamamoto, Kinetic theory with Berry curvature from quantum field theories, *Phys. Rev.* **D87**, 085016 (2013), [doi:10.1103/PhysRevD.87.085016](https://doi.org/10.1103/PhysRevD.87.085016).
- [89] J.-W. Chen, S. Pu, Q. Wang, and X.-N. Wang, Berry Curvature and Four-Dimensional Monopoles in the Relativistic Chiral Kinetic Equation, *Phys. Rev. Lett.* **110**, 262301 (2013), [doi:10.1103/PhysRevLett.110.262301](https://doi.org/10.1103/PhysRevLett.110.262301).
- [90] C. Manuel and J. M. Torres-Rincon, Kinetic theory of chiral relativistic plasmas and energy density of their gauge collective excitations, *Phys. Rev.* **D89**, 096002 (2014), [doi:10.1103/PhysRevD.89.096002](https://doi.org/10.1103/PhysRevD.89.096002).
- [91] C. Manuel and J. M. Torres-Rincon, Chiral transport equation from the quantum Dirac Hamiltonian and the on-shell effective field theory, *Phys. Rev.* **D90**, 076007 (2014), [doi:10.1103/PhysRevD.90.076007](https://doi.org/10.1103/PhysRevD.90.076007).
- [92] J.-Y. Chen, D. T. Son, M. A. Stephanov, H.-U. Yee, and Y. Yin, Lorentz Invariance in Chiral Kinetic Theory, *Phys. Rev. Lett.* **113**, 182302 (2014), [doi:10.1103/PhysRevLett.113.182302](https://doi.org/10.1103/PhysRevLett.113.182302).
- [93] J.-Y. Chen, D. T. Son, and M. A. Stephanov, Collisions in Chiral Kinetic Theory, *Phys. Rev. Lett.* **115**, 021601 (2015), [doi:10.1103/PhysRevLett.115.021601](https://doi.org/10.1103/PhysRevLett.115.021601).
- [94] Y. Hidaka, S. Pu, and D.-L. Yang, Relativistic Chiral Kinetic Theory from Quantum Field Theories, *Phys. Rev.* **D95**, 091901 (2017), [doi:10.1103/PhysRevD.95.091901](https://doi.org/10.1103/PhysRevD.95.091901).
- [95] N. Mueller and R. Venugopalan, The chiral anomaly, Berry's phase and chiral kinetic theory, from world-lines in quantum field theory, *Phys. Rev.* **D97**, 051901 (2018), [doi:10.1103/PhysRevD.97.051901](https://doi.org/10.1103/PhysRevD.97.051901).
- [96] Y. Hidaka, S. Pu, and D.-L. Yang, Nonlinear Responses of Chiral Fluids from Kinetic Theory, *Phys. Rev.* **D97**, 016004 (2018), [doi:10.1103/PhysRevD.97.016004](https://doi.org/10.1103/PhysRevD.97.016004).
- [97] Y. Hidaka, S. Pu, and D.-L. Yang, Non-Equilibrium Quantum Transport of Chiral Fluids from Kinetic Theory, *Nucl. Phys.* **A982**, 547 (2019), [doi:10.1016/j.nuclphysa.2018.10.033](https://doi.org/10.1016/j.nuclphysa.2018.10.033).
- [98] A. Huang, S. Shi, Y. Jiang, J. Liao, and P. Zhuang, Complete and Consistent Chiral Transport from Wigner Function Formalism, *Phys. Rev.* **D98**, 036010 (2018), [doi:10.1103/PhysRevD.98.036010](https://doi.org/10.1103/PhysRevD.98.036010).
- [99] J.-H. Gao, Z.-T. Liang, Q. Wang, and X.-N. Wang, Disentangling covariant Wigner functions for chiral fermions, *Phys. Rev.* **D98**, 036019 (2018), [doi:10.1103/PhysRevD.98.036019](https://doi.org/10.1103/PhysRevD.98.036019).
- [100] Y.-C. Liu, L.-L. Gao, K. Mameda, and X.-G. Huang, Chiral kinetic theory in curved spacetime, *Phys. Rev.* **D99**, 085014 (2019), [doi:10.1103/PhysRevD.99.085014](https://doi.org/10.1103/PhysRevD.99.085014).
- [101] S. Lin and A. Shukla, Chiral Kinetic Theory from Effective Field Theory Revisited, *JHEP* **06**, 060 (2019), [doi:10.1007/JHEP06\(2019\)060](https://doi.org/10.1007/JHEP06(2019)060).
- [102] S. Lin and L. Yang, Chiral kinetic theory from Landau level basis, *Phys. Rev. D* **101**, 034006 (2020), [doi:10.1103/PhysRevD.101.034006](https://doi.org/10.1103/PhysRevD.101.034006).
- [103] Y. Sun, C. M. Ko, and F. Li, Anomalous transport model study of chiral magnetic effects in heavy ion collisions, *Phys. Rev.* **C94**, 045204 (2016), [doi:10.1103/PhysRevC.94.045204](https://doi.org/10.1103/PhysRevC.94.045204).
- [104] Y. Sun and C. M. Ko, Chiral vortical and magnetic effects in the anomalous transport model, *Phys. Rev.* **C95**, 034909 (2017), [doi:10.1103/PhysRevC.95.034909](https://doi.org/10.1103/PhysRevC.95.034909).
- [105] Y. Sun and C. M. Ko, A hyperon polarization in relativistic heavy ion collisions from a chiral kinetic approach, *Phys. Rev.* **C96**, 024906 (2017), [doi:10.1103/PhysRevC.96.024906](https://doi.org/10.1103/PhysRevC.96.024906).

- [106] Y. Sun and C. M. Ko, Chiral kinetic approach to the chiral magnetic effect in isobaric collisions, Phys. Rev. **C98**, 014911 (2018), doi:10.1103/PhysRevC.98.014911.
- [107] Y. Sun and C. M. Ko, Azimuthal angle dependence of the longitudinal spin polarization in relativistic heavy ion collisions, Phys. Rev. **C99**, 011903 (2019), doi:10.1103/PhysRevC.99.011903.
- [108] W.-H. Zhou and J. Xu, Simulating the Chiral Magnetic Wave in a Box System, Phys. Rev. **C98**, 044904 (2018), doi:10.1103/PhysRevC.98.044904.
- [109] W.-H. Zhou and J. Xu, Simulating chiral anomalies with spin dynamics, Phys. Lett. **B798**, 134932 (2019), doi:10.1016/j.physletb.2019.134932.
- [110] S. Y. F. Liu, Y. Sun, and C. M. Ko, Spin polarizations in a covariant angular momentum conserved chiral transport model, in preparation, arXiv:1910.06774.
- [111] STAR, J. Adam *et al.*, Global polarization of Λ hyperons in Au+Au collisions at $\sqrt{s_{NN}} = 200$ GeV, Phys. Rev. **C98**, 014910 (2018), doi:10.1103/PhysRevC.98.014910.
- [112] J.-H. Gao and Z.-T. Liang, Relativistic Quantum Kinetic Theory for Massive Fermions and Spin Effects, Phys. Rev. **D100**, 056021 (2019), doi:10.1103/PhysRevD.100.056021.
- [113] N. Weickgenannt, X.-L. Sheng, E. Speranza, Q. Wang, and D. H. Rischke, Kinetic theory for massive spin-1/2 particles from the Wigner-function formalism, Phys. Rev. D **100**, 056018 (2019), doi:10.1103/PhysRevD.100.056018.
- [114] N. Weickgenannt, X.-L. Sheng, E. Speranza, Q. Wang, and D. H. Rischke, Wigner function and kinetic theory for massive spin-1/2 particles, in *28th International Conference on Ultrarelativistic Nucleus-Nucleus Collisions (Quark Matter 2019) Wuhan, China, November 4-9, 2019*, in preparation, arXiv:2001.11862.
- [115] U. W. Heinz, Kinetic Theory for Nonabelian Plasmas, Phys. Rev. Lett. **51**, 351 (1983), doi:10.1103/PhysRevLett.51.351.
- [116] H. T. Elze, M. Gyulassy, and D. Vasak, Transport Equations for the QCD Quark Wigner Operator, Nucl. Phys. **B276**, 706 (1986), doi:10.1016/0550-3213(86)90072-6.
- [117] D. Vasak, M. Gyulassy, and H. T. Elze, Quantum Transport Theory for Abelian Plasmas, Annals Phys. **173**, 462 (1987), doi:10.1016/0003-4916(87)90169-2.
- [118] J.-H. Gao, Z.-T. Liang, and Q. Wang, Dirac sea and chiral anomaly in the quantum kinetic theory, (2019), 1910.11060.
- [119] X.-L. Sheng, Q. Wang, and X.-G. Huang, Kinetic theory with spin: From massive to massless fermions, in preparation, arXiv:2005.00204.
- [120] K. Hattori, Y. Hidaka, and D.-L. Yang, Axial Kinetic Theory and Spin Transport for Fermions with Arbitrary Mass, Phys. Rev. **D100**, 096011 (2019), doi:10.1103/PhysRevD.100.096011.
- [121] D.-L. Yang, K. Hattori, and Y. Hidaka, Quantum kinetic theory for spin transport: general formalism for collisional effects, in preparation, arXiv:2002.02612.
- [122] Y.-C. Liu, K. Mameda, and X.-G. Huang, Covariant Spin Kinetic Theory I: Collisionless Limit, in preparation, arXiv:2002.03753.
- [123] I. Bialynicki-Birula, P. Gornicki, and J. Rafelski, Phase space structure of the Dirac vacuum, Phys. Rev. D **44**, 1825 (1991), doi:10.1103/PhysRevD.44.1825.
- [124] P.-f. Zhuang and U. W. Heinz, Equal-Time Hierarchies in Quantum Transport Theory, Phys. Rev. D **57**, 6525 (1998), doi:10.1103/PhysRevD.57.6525.
- [125] E. Gorbar, V. Miransky, I. Shovkovy, and P. Sukhachov, Wigner function and kinetic phenomena for chiral plasma in a strong magnetic field, JHEP **08**, 103 (2017), doi:10.1007/JHEP08(2017)103.
- [126] F. Hebenstreit, R. Alkofer, and H. Gies, Schwinger pair production in space and time-dependent electric fields: Relating the Wigner formalism to quantum kinetic theory, Phys. Rev. D **82**, 105026 (2010), doi:10.1103/PhysRevD.82.105026.
- [127] X.-L. Sheng, R.-H. Fang, Q. Wang, and D. H. Rischke, Wigner function and pair production in parallel electric and magnetic fields, Phys. Rev. **D99**, 056004 (2019), doi:10.1103/PhysRevD.99.056004.
- [128] Z. Wang, X. Guo, S. Shi, and P. Zhuang, Mass Correction to Chiral Kinetic Equations, Phys. Rev. **D100**, 014015 (2019), doi:10.1103/PhysRevD.100.014015.
- [129] S. Li and H.-U. Yee, Quantum Kinetic Theory of Spin Polarization of Massive Quarks in Perturbative QCD: Leading Log, Phys. Rev. **D100**, 056022 (2019), doi:10.1103/PhysRevD.100.056022.
- [130] X. Guo, Massless Limit of Transport Theory for Massive Fermions,
- [131] Z.-T. Liang and X.-N. Wang, Globally polarized quark-gluon plasma in non-central A+A collisions, Phys. Rev. Lett. **94**, 102301 (2005), doi: 10.1103/PhysRevLett.94.102301, [Erratum: Phys. Rev. Lett.96,039901(2006)]. doi:10.1103/PhysRevLett.96.039901.
- [132] Z.-T. Liang and X.-N. Wang, Spin alignment of vector mesons in non-central A+A collisions, Phys. Lett. **B629**, 20 (2005), doi:10.1016/j.physletb.2005.09.060.
- [133] B. Betz, M. Gyulassy, and G. Torrieri, Polarization probes of vorticity in heavy ion collisions, Phys. Rev. C **76**, 044901 (2007), doi:10.1103/PhysRevC.76.044901.
- [134] F. Becattini and F. Piccinini, The Ideal relativistic spinning gas: Polarization and spectra, Annals Phys. **323**, 2452 (2008), doi:10.1016/j.aop.2008.01.001.
- [135] F. Becattini, F. Piccinini, and J. Rizzo, Angular momentum conservation in heavy ion collisions at very high energy, Phys. Rev. C **77**, 024906 (2008), doi:10.1103/PhysRevC.77.024906.
- [136] F. Becattini, V. Chandra, L. Del Zanna, and E. Grossi, Relativistic distribution function for particles with spin at local thermodynamical equilibrium, Annals Phys. **338**, 32 (2013), doi:10.1016/j.aop.2013.07.004.
- [137] Q. Wang, Global and local spin polarization in heavy ion collisions: a brief overview, Nucl. Phys. A **967**, 225 (2017), doi:10.1016/j.nuclphysa.2017.06.053.
- [138] F. Becattini and M. A. Lisa, Polarization and Vorticity in the Quark Gluon Plasma, (2020), doi:10.1146/annurev-nucl-021920-095245.
- [139] F. Becattini, Polarization in relativistic fluids: a quantum field theoretical derivation, in preparation, arXiv:2004.04050.

- [140] Y. Jiang, Z.-W. Lin, and J. Liao, Rotating quark-gluon plasma in relativistic heavy ion collisions, *Phys. Rev.* **C94**, 044910 (2016), doi:10.1103/PhysRevC.94.044910, [Erratum: *Phys. Rev.* C95,no.4,049904(2017)], doi:10.1103/PhysRevC.95.049904.
- [141] W.-T. Deng and X.-G. Huang, Vorticity in Heavy-Ion Collisions, *Phys. Rev.* **C93**, 064907 (2016), doi:10.1103/PhysRevC.93.064907.
- [142] H. Li, L.-G. Pang, Q. Wang, and X.-L. Xia, Global Λ polarization in heavy-ion collisions from a transport model, *Phys. Rev. C* **96**, 054908 (2017), doi:10.1103/PhysRevC.96.054908.
- [143] D.-X. Wei, W.-T. Deng, and X.-G. Huang, Thermal vorticity and spin polarization in heavy-ion collisions, *Phys. Rev. C* **99**, 014905 (2019), doi:10.1103/PhysRevC.99.014905.
- [144] L. Csernai, V. Magas, and D. Wang, Flow Vorticity in Peripheral High Energy Heavy Ion Collisions, *Phys. Rev. C* **87**, 034906 (2013), doi:10.1103/PhysRevC.87.034906.
- [145] F. Becattini, L. Csernai, and D. Wang, Λ polarization in peripheral heavy ion collisions, *Phys. Rev. C* **88**, 034905 (2013), [Erratum: *Phys.Rev.C* 93, 069901 (2016)], doi:10.1103/PhysRevC.88.034905.
- [146] F. Becattini *et al.*, A study of vorticity formation in high energy nuclear collisions, *Eur. Phys. J. C* **75**, 406 (2015), [Erratum: *Eur.Phys.J.C* 78, 354 (2018)], doi:10.1140/epjc/s10052-015-3624-1.
- [147] L.-G. Pang, H. Petersen, Q. Wang, and X.-N. Wang, Vortical Fluid and Λ Spin Correlations in High-Energy Heavy-Ion Collisions, *Phys. Rev. Lett.* **117**, 192301 (2016), doi:10.1103/PhysRevLett.117.192301.
- [148] H.-Z. Wu, L.-G. Pang, X.-G. Huang, and Q. Wang, Local spin polarization in high energy heavy ion collisions, *Phys. Rev. Research.* **1**, 033058 (2019), doi:10.1103/PhysRevResearch.1.033058.
- [149] H.-Z. Wu, L.-G. Pang, X.-G. Huang, and Q. Wang, Local Spin Polarization in 200 GeV Au+Au and 2.76 TeV Pb+Pb Collisions, in *28th International Conference on Ultrarelativistic Nucleus-Nucleus Collisions*, in preparation, arXiv:2002.03360.
- [150] Y. B. Ivanov and A. A. Soldatov, Vorticity in heavy-ion collisions at the JINR Nuclotron-based Ion Collider Facility, *Phys. Rev. C* **95**, 054915 (2017), doi:10.1103/PhysRevC.95.054915.
- [151] Y. B. Ivanov and A. A. Soldatov, Vortex rings in fragmentation regions in heavy-ion collisions at $\sqrt{s_{NN}} = 39$ GeV, *Phys. Rev. C* **97**, 044915 (2018), doi:10.1103/PhysRevC.97.044915.
- [152] Y. B. Ivanov, V. D. Toneev, and A. A. Soldatov, Estimates of hyperon polarization in heavy-ion collisions at collision energies $\sqrt{s_{NN}} = 4 - 40$ GeV, *Phys. Rev. C* **100**, 014908 (2019), doi:10.1103/PhysRevC.100.014908.
- [153] R.-h. Fang, J.-y. Pang, Q. Wang, and X.-n. Wang, Pseudoscalar condensation induced by chiral anomaly and vorticity for massive fermions, *Phys. Rev.* **D95**, 014032 (2017), doi:10.1103/PhysRevD.95.014032.
- [154] D. N. Zubarev, A. V. Prozorkevich, and S. A. Smolyanskii, Derivation of nonlinear generalized equations of quantum relativistic hydrodynamics, *Theoretical and Mathematical Physics* **40**, 821 (1979), doi:10.1007/BF01032069.
- [155] C. van Weert, Maximum entropy principle and relativistic hydrodynamics, *Annals of Physics* **140**, 133 (1982), doi:10.1016/0003-4916(82)90338-4.
- [156] F. Becattini, L. Bucciantini, E. Grossi, and L. Tinti, Local thermodynamical equilibrium and the beta frame for a quantum relativistic fluid, *Eur. Phys. J. C* **75**, 191 (2015), doi:10.1140/epjc/s10052-015-3384-y.
- [157] F. Becattini, W. Florkowski, and E. Speranza, Spin tensor and its role in non-equilibrium thermodynamics, *Physics Letters B* **789**, 419 (2019), doi:10.1016/j.physletb.2018.12.016.
- [158] E. Leader and C. Lorcé, The angular momentum controversy: What's it all about and does it matter?, *Phys. Rept.* **541**, 163 (2014), doi:10.1016/j.physrep.2014.02.010.
- [159] K. Fukushima and S. Pu, Relativistic decomposition of the orbital and the spin angular momentum in chiral physics and Feynman's angular momentum paradox, (2020), in preparation, arXiv:2001.00359.
- [160] K. Fukushima, S. Pu, and Z. Qiu, Eddy magnetization from the chiral Barnett effect, *Phys. Rev.* **A99**, 032105 (2019), doi:10.1103/PhysRevA.99.032105.
- [161] W. Florkowski, B. Friman, A. Jaiswal, and E. Speranza, Relativistic fluid dynamics with spin, *Phys. Rev. C* **97**, 041901 (2018), doi:10.1103/PhysRevC.97.041901.
- [162] W. Florkowski, E. Speranza, and F. Becattini, Perfect-fluid hydrodynamics with constant acceleration along the stream lines and spin polarization, *Acta Phys. Polon. B* **49**, 1409 (2018), doi:10.5506/APhysPolB.49.1409.
- [163] W. Florkowski, R. Ryblewski, and A. Kumar, Relativistic hydrodynamics for spin-polarized fluids, *Prog. Part. Nucl. Phys.* **108**, 103709 (2019), doi:10.1016/j.pnpnp.2019.07.001.
- [164] K. Hattori, M. Hongo, X.-G. Huang, M. Matsuo, and H. Taya, Fate of spin polarization in a relativistic fluid: An entropy-current analysis, *Phys. Lett. B* **795**, 100 (2019), doi:10.1016/j.physletb.2019.05.040.
- [165] S. Bhadury, W. Florkowski, A. Jaiswal, A. Kumar, and R. Ryblewski, Relativistic dissipative spin dynamics in the relaxation time approximation, (2020), in preparation, arXiv:2002.03937.
- [166] D. Montenegro, L. Tinti, and G. Torrieri, Ideal relativistic fluid limit for a medium with polarization, *Phys. Rev. D* **96**, 056012 (2017), [Erratum: *Phys.Rev.D* 96, 079901 (2017)]. doi:10.1103/PhysRevD.96.056012.
- [167] D. Montenegro, L. Tinti, and G. Torrieri, Sound waves and vortices in a polarized relativistic fluid, *Phys. Rev. D* **96**, 076016 (2017), doi:10.1103/PhysRevD.96.076016.
- [168] D. Montenegro and G. Torrieri, Causality and dissipation in relativistic polarizable fluids, *Phys. Rev. D* **100**, 056011 (2019), doi:10.1103/PhysRevD.100.056011.
- [169] D. Montenegro and G. Torrieri, Linear response theory of relativistic hydrodynamics with spin, in preparation, arXiv:2004.10195.
- [170] S. R. De Groot, *Relativistic Kinetic Theory. Principles and Applications* (, 1980).
- [171] J.-j. Zhang, R.-h. Fang, Q. Wang, and X.-N. Wang, A microscopic description for polarization in particle scatterings, *Phys. Rev. C* **100**, 064904 (2019), doi:10.1103/PhysRevC.100.064904.
- [172] H.-Z. Wu, J.-J. Zhang, L.-G. Pang, and Q. Wang, ZMCintegral: A package for multi-dimensional Monte Carlo integration on multi-GPUs, *Computer Physics Communications* **248**, 106962 (2020), doi:10.1016/j.cpc.2019.106962.

- [173] J.-J. Zhang and H.-Z. Wu, ZMCintegral-v5: Support for Integrations with the scanning of large parameter space on multi-GPUs, *Computer Physics Communications* , 107240 (2020), doi:10.1016/j.cpc.2020.107240.
- [174] J.-J. Zhang, H.-Z. Wu, S. Pu, G.-Y. Qin, and Q. Wang, Towards a full solution of relativistic Boltzmann equation for quark-gluon matter on GPUs, (2019), in preparation, arXiv:1912.04457.
- [175] N. Weickgenannt, E. Speranza, X.-l. Sheng, Q. Wang, and D. H. Rischke, Generating spin polarization from vorticity through nonlocal collisions, (2020), in preparation, arXiv:2005.01506.
- [176] F. Becattini, I. Karpenko, M. A. Lisa, I. Upsal, and S. A. Voloshin, Global hyperon polarization at local thermodynamic equilibrium with vorticity, magnetic field, and feed-down, *Phys. Rev. C* **95**, 054902 (2017), doi:10.1103/PhysRevC.95.054902.
- [177] L. Csernai, J. Kapusta, and T. Welle, Λ and $\bar{\Lambda}$ spin interaction with meson fields generated by the baryon current in high energy nuclear collisions, *Phys. Rev. C* **99**, 021901 (2019), doi:10.1103/PhysRevC.99.021901.
- [178] X. Guo, J. Liao, and E. Wang, Magnetic Field in the Charged Subatomic Swirl, *Sci. Rep.* **10**, 2196 (2020), doi:10.1038/s41598-020-59129-6.
- [179] I. Karpenko and F. Becattini, Study of Λ polarization in relativistic nuclear collisions at $\sqrt{s_{NN}} = 7.7-200$ GeV, *The European Physical Journal C* **77**, 213 (2017), doi:0.1140/epjc/s10052-017-4765-1.
- [180] Y. Xie, D. Wang, and L. P. Csernai, Global Λ polarization in high energy collisions, *Phys. Rev. C* **95**, 031901 (2017), doi:10.1103/PhysRevC.95.031901.
- [181] S. Shi, K. Li, and J. Liao, Searching for the subatomic swirls in the CuCu and CuAu collisions, *Physics Letters B* **788**, 409 (2019), doi:10.1016/j.physletb.2018.09.066.
- [182] F. Becattini and I. Karpenko, Collective Longitudinal Polarization in Relativistic Heavy-Ion Collisions at Very High Energy, *Phys. Rev. Lett.* **120**, 012302 (2018), doi:10.1103/PhysRevLett.120.012302.
- [183] X.-L. Xia, H. Li, Z.-B. Tang, and Q. Wang, Probing vorticity structure in heavy-ion collisions by local Λ polarization, *Phys. Rev. C* **98**, 024905 (2018), doi:10.1103/PhysRevC.98.024905.
- [184] Voloshin, Sergei A., Vorticity and particle polarization in heavy ion collisions (experimental perspective), *EPJ Web Conf.* **171**, 07002 (2018), doi:10.1051/epjconf/201817107002.
- [185] X.-L. Xia, H. Li, X.-G. Huang, and H. Z. Huang, Feed-down effect on Λ spin polarization, *Phys. Rev. C* **100**, 014913 (2019), doi:10.1103/PhysRevC.100.014913.
- [186] F. Becattini, G. Cao, and E. Speranza, Polarization transfer in hyperon decays and its effect in relativistic nuclear collisions, *The European Physical Journal C* **79**, 741 (2019), doi:10.1140/epjc/s10052-019-7213-6.
- [187] K. Schilling, P. Seyboth, and G. E. Wolf, On the Analysis of Vector Meson Production by Polarized Photons, *Nucl. Phys.* **B15**, 397 (1970), doi:10.1016/0550-3213(70)90070-2, [Erratum: *Nucl. Phys.*B18,332(1970)],doi:10.1016/0550-3213(70)90295-6.
- [188] STAR, B. I. Abelev *et al.*, Spin alignment measurements of the $K^*(892)$ and $\phi(1020)$ vector mesons in heavy ion collisions at $s_{NN}^{1/2} = 200$ GeV, *Phys. Rev. C* **77**, 061902 (2008), doi:10.1103/PhysRevC.77.061902.
- [189] ALICE, S. Acharya *et al.*, Measurement of spin-orbital angular momentum interactions in relativistic heavy-ion collisions, in preparation, arXiv:1910.14408.
- [190] Y.-G. Yang, R.-H. Fang, Q. Wang, and X.-N. Wang, Quark coalescence model for polarized vector mesons and baryons, *Phys. Rev. C* **97**, 034917 (2018), doi:10.1103/PhysRevC.97.034917.
- [191] X.-L. Sheng, L. Oliva, and Q. Wang, What can we learn from global spin alignment of ϕ meson in heavy-ion collisions?, in preparation, arXiv:1910.13684.